Dampened α7 nAChR activity contributes to audiogenic seizures and hyperactivity in a mouse model of Fragile X Syndrome

Sarah Goebel[1], Dylann Cordova-Martinez[1], Vytas K. Verselis[1†], Anna Francesconi[1†*]

[1]Department of Neuroscience, Albert Einstein College of Medicine; New York, NY, U.S.A

*Corresponding author. Email: anna.francesconi@einsteinmed.edu

† These authors contributed equally to this work.

Abstract: Fragile X Syndrome (FXS) is the most common form of inherited intellectual disability and often accompanied with debilitating pathologies including seizures and hyperactivity. FXS arises from a trinucleotide repeat expansion in the 5' UTR of the *FMR1* gene that silences expression of the RNA-binding protein FMRP. Despite progress in understanding FMRP functions, the identification of effective therapeutic targets has lagged and at present there are no viable treatment options. Here we identify the α7 nicotinic acetylcholine receptor (nAChR) as candidate target for intervention in FXS. In the early postnatal hippocampus of *Fmr1* knockout (KO) mice, an established pre-clinical model of FXS, the α7 nAChR accessory protein Ly6H is abnormally enriched at the neuronal surface and mislocalized in dendrites. Ly6H, a GPI-anchored protein, binds α7 nAChRs with high affinity and can limit α7 nAChR surface expression and signaling. We find that α7 nAChR-evoked Ca^{2+} responses are dampened

in immature glutamatergic and GABAergic *Fmr1*^{KO} neurons compared to wild type. Knockdown of endogenous Ly6H in *Fmr1*^{KO} neurons is sufficient to rescue dampened α7 nAChR Ca^{2+} responses in vitro, providing evidence of a cell-autonomous role for Ly6H aberrant expression in α7 nAChR hypofunction. In line with intrinsic deficits in α7 nAChR activity in *Fmr1*^{KO} neurons, in vivo administration of the α7 nAChR-selective positive allosteric modulator PNU-120596 reduced hyperactivity and seizure severity in adolescent *Fmr1*^{KO} mice. Our mechanistic studies together with evidence of the in vivo efficacy of α7 nAChR augmentation implicate α7 nAChR hypofunction in FXS pathology.

Summary: Correction of α7 nAChR hypofunction in a preclinical murine model of Fragile X syndrome ameliorates seizure severity and hyperactivity.

INTRODUCTION

Fragile X Syndrome (FXS) is the most prevalent form of inherited intellectual disability with approximately 1/7,000 males and 1/11,000 females diagnosed (*1*). FXS is often co-morbid with associated pathologies including seizures in infancy (~ 18% of males, 7% females), attention deficit hyperactivity (~ 80%) and autism (~ 30%) (*2, 3*). FXS arises from the abnormal expansion of a trinucleotide repeat in the 5' UTR of the X-linked *FMR1* gene resulting in its silencing by hypermethylation and global loss of expression of the encoded Fragile X messenger ribonucleoprotein (FMRP) (*4, 5*). FMRP is an RNA-binding protein that regulates translation, trafficking and stability of ~8% of brain-expressed RNAs (*5*). Studies utilizing the *Fmr1* knockout (KO) mouse have revealed that loss of FMRP is associated with dendritic spine

dysgenesis, deficits in forms of synaptic plasticity, and hyperexcitability (*6*). Despite remarkable progress in understanding cellular and synaptic dysfunctions arising from *FMR1* silencing, there are currently no treatment options for patients beyond palliative measures, underscoring the urgent need to identify avenues for early therapeutic intervention.

Acetylcholine (ACh) is a potent neuromodulator/neurotransmitter that through widespread cholinergic fiber innervation plays an important role in regulating critical periods of brain development driven by sensory and experience-dependent activity (*7-9*). ACh actions are mediated in part by nicotinic ACh receptors (nAChRs), a family of ligand-gated ion channels broadly expressed in the CNS. Amongst nAChRs, activation of the homopentameric α7 nAChRs during early postnatal development crucially contributes to the maturation of excitatory and inhibitory neurons and their synapses, and the formation of neural networks (*8-12*). Although alterations in signaling by G protein coupled muscarinic ACh receptors were reported in *Fmr1*^{KO} mice (*13, 14*), whether α7 nAChR activity is compromised in FXS remains untested despite evidence of its role in many of the processes that go awry in individuals with FXS including seizures, hyperactivity and hypersensitivity to sensory stimuli (*15-20*). The critical impact of α7 nAChRs on neuronal function/maturation is attributable to its high Ca^{2+} permeability (*21*) that can initiate downstream signaling and affect neurotransmitter release. Tight control of α7 nAChR activity is essential to limit excessive cytotoxic Ca^{2+} influx and is achieved in part through regulated biogenesis and surface export (*22*). The glycosylphosphatidylinositol (GPI)-anchored Ly6/uPAR proteins are an integral component of the nAChR signaling unit (*23*). They specifically bind to nAChRs *via* a three-finger domain structurally related to that of α-bungarotoxin which binds nAChRs with high affinity (*23*). Seminal studies established a role of members of the Ly6/uPAR protein family as endogenous modulators of nAChR activity in the

CNS by enhancing receptor desensitization and reducing surface expression (*24-26*). We previously reported a genome wide proteomic screen of the adult *Fmr1*^{KO} mouse brain that found Lymphocyte Antigen 6 Family Member H (Ly6H), a member of the Ly6/uPAR family, to be selectively depleted from membrane fractions containing lipid rafts (*27*). Ly6H, a brain enriched protein expressed in neurons, is of particular interest as it binds to and regulates α7 nAChR function by limiting its surface expression (*25, 28*) and by restraining its activity through direct interaction at the plasma membrane (*29*).

In this study, we report that Ly6H surface expression is aberrantly elevated, showing relatively increased expression in soma and dendrites of immature hippocampal *Fmr1*^{KO} neurons. Concomitant with altered Ly6H expression and congruent with its functions, we find reduced evoked responses of α7 nAChRs in *Fmr1*^{KO} hippocampal neurons of both glutamatergic and GABAergic lineage that can be corrected by downregulation of Ly6H. We further demonstrate that early pharmacological enhancement of α7 nAChR activity in vivo reduces the severity of audiogenic seizures and hyperactivity in adolescent *Fmr1*^{KO} mice. Our results identify α7 nAChR hypofunction as a critical deficit arising from loss of FMRP and provide support for the therapeutic benefits of augmenting α7 nAChR activity in FXS.

RESULTS

Ly6H surface expression is increased in *Fmr1*^{KO} hippocampal neurons

In previous work, we used isobaric tags (iTRAQ) and mass spectrometry in adult wild type (WT) and *Fmr1*^{KO} forebrain to characterize the protein composition of detergent resistant membranes (DRM) that contain lipid rafts (*27*). Unlike most other GPI-anchored proteins identified in the screen, Ly6H (Fig. 1A) was found to be depleted in DRM from cortex and

hippocampus of *Fmr1*^{KO} mice relative to WT without substantial changes in total protein levels. GPI-anchored proteins are normally transported to and retained in lipid rafts and therefore the altered membrane distribution of Ly6H suggested potential defects in its trafficking and/or cellular localization. Thus, we examined Ly6H surface expression in the *Fmr1*^{KO} hippocampus at early postnatal ages when Ly6H begins to be expressed, becoming relatively abundant by postnatal day 7 (P7) (fig. S1). Freshly prepared hippocampal tissue slices from WT and *Fmr1*^{KO} P7-8 pups were live labeled with biotin and surface expressed biotinylated proteins were precipitated with immobilized streptavidin and analyzed by Western blot (Fig. 1B). The proportion of surface expressed Ly6H proved to be upregulated in *Fmr1*^{KO} hippocampus with mean 2.3-fold increase relative to WT, notwithstanding comparable total Ly6H abundance between genotypes (Fig. 1, B to C). Transcriptional RNA-sequencing (RNA-seq) profiles in single cells from adult murine and human brain demonstrate that Ly6H mRNA is predominantly expressed in neurons, including principal neurons in all subregions of the hippocampus (*30-32*). To visualize Ly6H protein expression in the intact hippocampus, Ly6H^{+} cells were immunolabeled in transverse hippocampal slices of WT and *Fmr1*^{KO} littermates at P7 and P22. At both ages, Ly6H immunofluorescence appeared punctate in both the pyramidal cell layer, marked by nuclear labeling with DAPI, and the neuropil (Fig. 1D). In the *Fmr1*^{KO}, Ly6H immunolabeling was higher in the CA1 pyramidal layer compared to WT (Fig. 1E) and denser in the proximal region of the *stratum radiatum* (extending 40 μm from the pyramidal layer) (Fig. 1F) that harbors the apical dendrites of pyramidal neurons.

To more closely examine Ly6H localization in dendrites, we used *Fmr1*^{KO} and WT primary hippocampal neurons which develop a complex dendritic arbor by 7 days in vitro (d.i.v.). This strategy allowed application of Ly6H antibody to non-permeabilized cells to

visualize surface Ly6H followed by post-permeabilization immunolabeling for the dendritic marker MAP2. Both the soma and the dendritic arbor were studded with Ly6H puncta in both genotypes (Fig. 1, G to H) but the Ly6H labeled area was ~1.5-fold greater in the *Fmr1*^{KO} soma compared to WT (Fig. 1I). Notably, Ly6H^{+} puncta appeared unevenly distributed in *Fmr1*^{KO} dendrites and more densely concentrated within 10 μm from the soma compared to WT (Fig. 1, H and J). As observed in hippocampal slices, total Ly6H protein abundance in primary hippocampal neurons was comparable between genotypes (fig. S2). Together these findings indicate that Ly6H, an accessory protein to α7 nAChR, is abnormally concentrated at the neuronal surface of immature *Fmr1*^{KO} hippocampal neurons.

Evoked α7 nAChR calcium responses are dampened in *Fmr1*^{KO} neurons

Ly6H was previously shown to reduce α7 nAChR surface expression by acting antagonistically to the α7-specific chaperone NACHO which facilitates α7 nAChR export from the endoplasmic reticulum (*28*). Notably, Ly6H was also shown to directly restrain α7 nAChR activity at the plasma membrane through its association with the extracellular face of the mature homopentamer (*29*). These key properties of Ly6H prompted us to consider the possibility that its aberrant localization in *Fmr1*^{KO} neurons may lead to intrinsically altered α7 nAChR activity. The α7 nAChR is one of the most abundant nAChRs in the brain and predominant in the hippocampus where its expression peaks in the first two postnatal weeks in rodents (*33, 34*). α7 nAChR is expressed in excitatory neurons and enriched in GABAergic cells both during their early maturation, when GABA is excitatory, and in mature interneurons (*33, 35, 36*). To examine α7 nAChR responses, we took advantage of its high Ca^{2+} permeability (in hippocampal neurons P_{Ca}/P_{Na} 6.1) and the availability of selective positive allosteric modulators (PAMs) which inhibit

its rapid desensitization (*21*). α7 nAChR responses were first examined in primary WT hippocampal neurons loaded with the ratiometric Ca^{2+} indicator Fura-2 AM and evoked by bath application of the specific α7 agonist PNU-282987 (100 nM) (*37*) together with the PAM PNU-120596 (3 μM) (*20*). Neurons were maintained in tetrodotoxin (0.5 μM) and atropine (1 μM) during the recordings to block Na^{+} channels and muscarinic ACh receptors, respectively. Stimulation with the agonist produced a rapid raise in intracellular Ca^{2+} (Fig. 2, A to B) that was blocked by the α7 nAChR-selective antagonist methyllycaconitine (MLA, 10 nM), confirming that responses were mediated by α7 nAChRs (Fig. 2C). Because the magnitude of the responses varied across cells and since α7 nAChRs are expressed in both GABAergic and glutamatergic neurons, both present in the primary cultures, post-hoc immunolabeling of glutamic acid decarboxylase (GAD65) was used to identify GABAergic neurons (Fig. 2D). This procedure allowed us pair the Ca^{2+} responses with neurochemical signatures of each neuron (Fig. 2E). GAD65(+) cells exhibited substantially stronger Ca^{2+} responses compared to GAD65(-) glutamatergic cells as quantified by assessing both the peak amplitude (Fig. 2, F to G) and the integrated area of the response (Fig. 2, H to I), in agreement with previous reports of higher α7 nAChR activity in GABAergic neurons based on electrophysiological and α-bungarotoxin labeling data (*35, 38*).

Having defined the cell-type dependent profile of α7 nAChR responses, we next sought to characterize α7 nAChR activity in *Fmr1*^{KO} neurons while factoring in potential changes over the course of neuronal maturation. Hence α7 nAChR responses were measured in WT and *Fmr1*^{KO} hippocampal neurons at d.i.v. 5, 7, and 9, a time window encompassing the functional maturation of GABAergic cells from excitatory to inhibitory comparable to the time window of maturation *in situ (12, 39, 40)*. In WT GAD65(-) glutamatergic neurons, the integrated area (Fig.

3, A and B) and peak amplitude (Fig. 3, A and C) of the Ca^{2+} responses evoked by application of PNU-282987/PNU-120596 increased from d.i.v. 5 to 7 and remained elevated at d.i.v. 9. In contrast, *Fmr1*^{KO} GAD65(-) cells did not exhibit a sharp increase in Ca^{2+} responses at d.i v. 7 *versus* d.i.v. 5 (Fig. 3A), as determine by both integrated area and peak amplitude (Fig. 3, B to C), suggesting a delay in the typical progression of the α7 nAChR response. In addition, the α7 nAChR responses in *Fmr1*^{KO} glutamatergic neurons were dampened compared to WT, as shown by reduced integrated area (Fig. 3D) and peak amplitude (Fig. 3E) of the Ca^{2+} rise at d.i.v. 7 and 9.

Similarly to GAD65(-) cells, in WT GAD65(+) GABAergic cells α7 nAChR activity was potentiated at d.i.v. 7 relative to d.i.v. 5 and declined by d.i.v. 9 as shown by the integrated area of the response (Fig. 4, A to B). Although the peak amplitude of the evoked responses did not differ significantly (Fig. 4, A to C) there was a significant correlation between the integrated area and the extended duration of the response measured by a response decline index (Fig. 4D) (Spearman r -0.4709, n = 54 cells, p = 0.0003) calculated as the ratio of the integrated area for the first 100 sec, which typically encompassed the rise and peak of the response, and the entire duration of the response back to baseline. Notably, *Fmr1*^{KO} GAD65(+) cells did not exhibit transient potentiation of α7 nAChR responses (Fig. 4, A and B to C) that, however, showed a marked reduction in the integrated area compared to WT at d.i.v. 7 and 9 (Fig. 4E). This reduction in integrated area in the *Fmr1*^{KO} was not driven by a significant decrease in the peak amplitude (Fig. 4F) but rather by a reduced duration of the Ca^{2+} response (Fig. 4G). Overall, these data indicate that α7 nAChR signaling is dampened in *Fmr1*^{KO} glutamatergic and GABAergic neurons early during their maturation and that the timing of developmental changes in α7 nAChR signaling is altered in *Fmr1*^{KO} neurons.

Reducing Ly6H expression enhances α7 nAChR responses in *Fmr1*^{KO} neurons

Having established that α7 nAChR activity is weakened in *Fmr1*^{KO} neurons, we considered the possibility that expression of the receptor might be diminished since FMRP can regulate mRNA stability and/or translation. The total abundance of α7 in protein extracts from hippocampal neurons at d.i.v. 5, 7, and 9 did not differ between *Fmr1*^{KO} and WT (fig. S3) and likewise, α7 expression in early postnatal hippocampus (P8) was comparable between genotypes (fig. S3). Labeling with fluorescent α-bungarotoxin (BGTX), which binds selectively and with high affinity the α7 nAChR homopentamers, did not demonstrate detectable differences in the density of surface bound BGTX in WT and *Fmr1*^{KO} hippocampal neurons (fig. S4), indicating that neither the total expression of the α7 subunit nor the amount of receptor reaching the surface are substantially altered in *Fmr1*^{KO} neurons. As mentioned above, Ly6H can restrain α7 nAChR activity by directly binding to α7 nAChRs inserted in the plasma membrane (*29*). The reported inhibition of α7 nAChR function by Ly6H is similar to the action of Lynx1, the first member of the Ly6/uPAR family shown to bind to and inhibit nAChRs, operating as an endogenous "brake" for nAChR signaling (*24*). Because in *Fmr1*^{KO} neurons the dampening of evoked α7 nAChR responses is concomitant with increased surface expression of Ly6H, we considered the possibility that reducing Ly6H expression may potentiate receptor signaling in individual neurons. Thus, we infected *Fmr1*^{KO} hippocampal neurons at d.i.v. 2 with viruses encoding a reporter eGFP together with a previously tested Ly6H-specific shRNA or with scrambled control shRNA and examined them at d.i.v. 9 (Fig. 5A). Western blot analysis of neurons treated with Ly6H shRNA confirmed efficient downregulation of the endogenous protein compared to control shRNA-treated cells (fig. S5). Evoked α7 nAChR Ca^{2+} responses were induced by bath-application of agonist PNU-282987 together with the PAM PNU-120596 as described above in

eGFP+ neurons that were immunolabeled post-hoc for Ly6H and GABA (Fig. 5B) to confirm downregulation and distinguish GABAergic (GABA+) *versus* glutamatergic neurons (GABA-), respectively. In both GABA(-) (Fig. 5, C to D) and GABA(+) neurons (Fig.5, E to F) Ly6H knockdown resulted in α7 nAChR Ca^{2+} responses with larger integrated areas compared to neurons that received scrambled shRNA. Thus, lowering the expression of Ly6H can ameliorate the dampened α7 nAChR Ca^{2+} responses in *Fmr1*^{KO} neurons.

PNU-120596 decreases hyperactivity and seizure severity in *Fmr1*^{KO} mice

Hyperactivity is reported in ~ 80% of Fragile X patients and ~ 18% of male patients experience seizures. Hyperactivity and audiogenic seizures (AGS) are reproducibly reported to occur in *Fmr1*^{KO} mice, with susceptibility to AGS being the most robust and reproducible behavioral phenotype across strains and as such frequently used in preclinical drug studies of FXS (*41, 42*). Notably, compromised α7 nAChR signaling has been implicated in the development of hyperactivity and seizures in animal models and human subjects (*15-18, 43-46*). Given the cell intrinsic nature of deficits in evoked α7 nAChR responses in *Fmr1*^{KO} neurons, we hypothesized that enhancing α7 nAChR activity could improve hyperactivity and AGS outcomes in *Fmr1*^{KO} mice. To that end, the α7 nAChR-selective PAM PNU-120596 (3 mg/kg) or vehicle was delivered by intraperitoneal injection (i.p.) to *Fmr1*^{KO} mice, with daily administration for five days starting at P18 and ending at P22 (Fig. 6A). Locomotor activity and audiogenic seizures (AGS) were sequentially assessed (in that order) ~ 8 hours after the last drug injection. Compared to the vehicle-treated, mice treated with PNU-120596 (Fig. 6B) exhibited a decrease in the total distance traveled (Fig. 6C), duration of movement (Fig. 6D) and the frequency of movement initiation (Fig. 6E). Next, mice were exposed to a loud alarm (~120 dB) for one

minute to trigger AGS initiation. AGS are generalized convulsive motor seizures triggered by acoustic stimulation that progress in several phases, starting from an initial period of wild running which can be followed by a tonic-clonic seizure and respiratory failure/cardiac arrest depending on seizure severity (fig. S6). In *Fmr1*^{KO} mice, AGS are reproducibly observed across ages and sexes with P22 being the most susceptible age (*41*). The progression and severity of AGS were scored according to an established metric, the Audiogenic Response Score (ARS) (fig. S6), that categorizes seizure severity from 1 to 9, with ARS 1 representing the least severe (wild running only). Administration of PNU-120596 reduced the severity of AGS compared to vehicle as indicated by less extreme ARS scores. A larger proportion of mice treated with PNU-120596 experienced two successive bouts of wild running (WR2) (Fig. 6F). The appearance of WR2 before presentation of a tonic-clonic phase indicates less severe seizure, as a continued amount of stimulation is required to set off potential seizure progression (*47, 48*). In aggregate, PNU-120596 administration resulted in less severe ARS scores, with a significant decrease in the percentage of mice that received an ARS score of 9 (Fig. 6G) and a higher percentage of mice with an ARS score of 4 and 8. Importantly, PNU-120596 reduced mortality following seizures (Fig. 6H). Overall, these results indicate that treatment with an α7 nAChR-selective positive allosteric modulator to counter α7 nAChR hypofunction reduces hyperactivity and the severity of seizures in a preclinical mouse model of FXS.

DISCUSSION

Our experimental results show that the trafficking of the α7 nAChR auxiliary protein Ly6H is altered in hippocampal *Fmr1*^{KO} neurons, resulting in aberrantly increased surface expression of Ly6H in proximal somatodendritic regions. Concomitantly, results also show that

Ca^{2+} responses in cultured hippocampal neurons evoked by application of an agonist for α7 nAChR are dampened in *Fmr1*^{KO} neurons of both glutamatergic and GABAergic lineage. The reduced evoked activity of α7 nAChRs in individual *Fmr1*^{KO} neurons could be potentiated by lowering Ly6H abundance, suggesting cell-intrinsic deficits in α7 nAChR responses contingent on mis-expression of Ly6H. In line with identified cellular deficits, in vivo administration of the bioactive positive allosteric modulator PNU-120596 - which increases evoked α7 nAChR-mediated Ca^{2+} influx - ameliorated two behavioral pathologies linked to abnormal hyperexcitability in *Fmr1*^{KO} mice (*6, 20*).

It is firmly established that both the expression of functional nAChRs and the strength and duration of their responses are the product of multiple highly regulated cellular processes, encompassing controlled biogenesis (*e.g*. folding, assembly), transport to the cell surface, and on-site modification of receptor properties. These processes are coordinated through cell-specific engagement of selective chaperone and auxiliary proteins and therefore dependent on their respective developmental and spatial profile of expression. The identification of these critical components of the "nAChR system" has provided key insights towards a more complete understanding of nAChR properties in pathophysiological conditions (*49*). Our results highlight Ly6H as one such critical component that could contribute to deficits in α7 nAChR function in *Fmr1*^{KO} neurons. Mechanistically, the observed alterations in Ly6H surface expression/localization may arise from aberrant processing of its GPI anchor and/or abnormalities in Golgi-plasma membrane transport. Indeed, several enzymes involved in the processing of GPI-anchored proteins are encoded by FMRP-client mRNAs (*50, 51*). In heterologous expression systems, Ly6H overexpression reduces α7 nAChR export to the surface and agonist binding, overall resulting in reduced evoked responses (*25*). Conversely,

downregulation of endogenous Ly6H was shown to boost α7 nAChR activity in rat hippocampal neurons (*25, 26*). However, Ly6H can also curb α7 nAChR responses by directly binding to the receptor itself when expressed in the plasma membrane, an effect abrogated by cleavage of the Ly6H GPI anchor or by mutations in 3-finger domain required for nAChR binding and structurally homologous to that of α-BGTX (*29*). CNS-expressed α7 nAChRs desensitize very rapidly and undergo prolonged residual inhibition (RID) (*34*). Several Ly6/uPAR family proteins have been shown to regulate nAChR desensitization either by accelerating (*e.g*. Lynx1, Lynx2) (*24, 52*) or delaying it (Ly6g6e) (*26*) resulting in net dampening or potentiation of the response, respectively. Endogenous Ly6H may reduce α7 nAChR activity in a membrane-delimited manner by promoting desensitization like Lynx1/2 proteins, so that abnormal crowding of Ly6H in somatodendritic regions of *Fmr1*^{KO} neurons could lead to locally depressed α7 nAChR responses. Our experimental results provide some support for this possibility since we did not detect reductions in α7 nAChR expression in *Fmr1*^{KO} neurons that could account for the dampened evoked responses. Moreover, downregulation of Ly6H expression was effective in boosting α7 nAChR activity.

Our results show a robust, but transient upregulation of α7 nAChR evoked activity during the early maturation of WT hippocampal neurons in vitro prior to the formation of excitatory synaptic contacts and the full maturation of interneurons. Notably, the transient increase in α7 nAChR activity - occurring at a time of heightened Ly6H mis-expression in mutant neurons - was compromised in the *Fmr1*^{KO}. Since the expression level of α7 subunits remained stable over time in both genotypes, these results suggest that the observed differences in the strength of α7 nAChR responses may depend on the regulated expression of α7 nAChR-associated proteins. Multiple members of the Ly6/uPAR family are expressed in hippocampal neurons (*53, 54*) and

their expression is developmentally regulated (*33*). Thus, potential competition between Ly6/uPAR proteins with opposing function (*e.g.* increasing *vs* decreasing nAChR desensitization) may contribute shaping the developmental progression of α7 nAChR responses. Aberrant expression of Ly6H mRNA was observed in FXS patient-derived iPSCs differentiated into dorsal forebrain neurons of glutamatergic lineage (*55*). Notably, Ly6H was found to be one of the most upregulated mRNAs in FXS neurons expressing glutamatergic phenotypes at late stages of in vitro differentiation, yet downregulated at early stages of differentiation (*55*). Interestingly, an independent study in FXS iPSC-derived immature neurons reported downregulation of Lynx1 (*56*). Thus, dysfunctions in nAChR auxiliary proteins that impact the maturation of functional nAChR responses are present in *Fmr1*^{KO} mice and FXS patients alike.

In the hippocampus, α7-nAChR signaling contributes to the maturation of excitatory and inhibitory neurons (*10, 12, 57*) and synapses (*11, 58*) both in vivo and in vitro as well as circuit formation/function during early postnatal development (*8, 12, 38*). Deficits in α7 nAChR signaling in *Fmr1*^{KO} neurons could be particularly impactful during critical periods of development when synaptic connectivity and neuronal networks are being formed and stabilized. The significantly more robust α7 nAChR responses that we experimentally observed in immature GABAergic cells suggest that α7 nAChRs could play a larger role in shaping inhibition, congruent with evidence of inhibitory deficits and interneuron dysfunction in FXS (*59*). nAChR auxiliary proteins such as Ly6H, Lynx1/2 and Lypd6 can associate with other nAChRs including α4β2 nAChR which is highly expressed in cortical regions. Thus, in addition to α7, other nAChRs may exhibit intrinsically altered activity in *Fmr1*^{KO} mice in a regional and cell-type specific manner. Our results indicate that aberrant trafficking of Ly6H and intrinsic deficits in α7 nAChR responses occur very early during hippocampal development (P7) and neuronal

maturation, respectively, ages that are relevant to FXS clinical manifestations (*60*). Most studies in *Fmr1*^{KO} mice have used juvenile or adult animals but recent evidence supports the notion that some cellular and synaptic pathologies in mutant mice may be compensatory and arise to mitigate primary deficits that originated during development (*61*). Related to this, enhanced cholinergic tone was reported in adult *Fmr1*^{KO} mice and linked to impaired attentional behavior (*62*). It will, thus, be important to define the temporal dynamics in FXS of expression of nAChR auxiliary proteins and intrinsic functional maturation of nAChRs, that might differ across brain regions and cell-type.

Alterations in muscarinic ACh receptor signaling and expression were also identified in *Fmr1*^{KO} mice (*13, 14*). Interestingly, despite upregulated expression of M1 and M4 receptors in *Fmr1*^{KO} mice, pharmacological enhancement of M4 activity with a PAM was found to be beneficial for amelioration of audiogenic seizures suggesting rescue of latent hypofunction. Our experimental results, together with the above-mentioned findings in *Fmr1*^{KO} mice and patients' derived cells, converge to suggest a broad cholinergic deficit in FXS. Deficits in cholinergic signaling have been reported in other neurodevelopmental disorders, such as Rett syndrome, demonstrated in both patient-derived neurons and a mouse model of the condition (*43, 63*). Moreover, cholinergic enhancement was shown to improve cognitive flexibility and social interaction in mouse models of autism and, congruent with preclinical studies, small open-label trials identified beneficial effects of targeting nAChRs in autism patients (*64*).

α7-nAChRs participate in many of the processes that go awry in individuals with FXS including seizures, hyperactivity, attention, and sleep. Independent studies reported early network hyperexcitability in *Fmr1*^{KO} mice (*65*). A prominent FXS pathology related to hyperexcitability is an increased susceptibility to seizures (*2*). *Fmr1*^{KO} mice are highly

susceptible to AGS - considered an expression of sensory hypersensitivity - a robust and reproducible phenotype that manifests at ~P17, peaks at ~P22 and persists into adulthood (*41*). Deletion of *Fmr1* in glutamatergic neurons in the inferior colliculus, where α7 nAChRs are expressed, is causally related to the manifestation of AGS in mutant mice. Our experimental results indicated that the timed, sustained delivery of PNU-120596 is effective in reducing AGS severity when their manifestation is most severe (P22). PNU-120596 may delay seizure progression or change seizure threshold by promoting the brain's natural dampening mechanisms. Although our results focused on α7 nAChR in hippocampal neurons, α7 and Ly6H are both widely expressed in the CNS suggesting that intrinsic dysfunctions in receptor activity might be present in different brain regions. About ~80% of FXS patients are diagnosed with attention-deficit hyperactivity disorder and, likewise, *Fmr1*^{KO} mice exhibit locomotor hyperactivity linked to circuit hyperexcitability. Our experimental results show that administration of PNU-120596 also ameliorates hyperlocomotion in adolescent *Fmr1*^{KO} mice, in agreement with previous work demonstrating that deficits in α7 nAChR signaling are causally related to manifestation of hyperactivity.

How can the results of our studies be translated to clinical interventions? As in any case, a primary requirement is the availability of safe and effective drugs. PNU-120596 is a type II PAM that inhibits α7 nAChR desensitization and enhances the potency of nicotinic agonists without activation of the receptors when administered alone. It is specific for α7 receptors, with no detectable effect on α4β2, α3β4 and α9α10 nAChRs, and has been shown to be bioactive and effective in many studies in rodents in which it is well tolerated. However, safety concerns because of potential excessive increase in $Ca2^{+}$ have prevented clinical testing. The type I PAM AVL-3288 could be considered as an alternative since it has been successfully evaluated for

safety and neurocognitive effects in healthy human subjects (*66*). Type I PAMs enhance α7 nAChR cholinergic activation but preserve its rapid desensitization, alleviating concerns of excessive Ca^{2+} influx. To move forward, preclinical studies could first establish dose and effectiveness of AVL-3288 in ameliorating hyperexcitability-related pathologies in *Fmr1*^{KO} mice and define the timing of interventions. A critical point would be to determine whether administration during a narrow temporal window early in development (*e.g.* P6-P14) could be sufficient for correction of deficits during adolescence or whether chronic or repeated treatment are instead needed. Nevertheless, given the lifelong persistence of FXS associated pathologies that are linked to α7 nAChR hypofunction, interventions with α7 PAMs are predicted to be also beneficial in adult subjects.

MATERIALS AND METHODS

Animals

WT and *Fmr1* KO (FVB.129P2-*Pde6b*$^{+}$ strain) mice were obtained from The Jackson Laboratories (Bar Harbor, ME) and bred in-house. Mice were fed ad libitum and housed with a 12 h light/dark cycle. All animal procedures were carried out according to protocols approved by the Albert Einstein College of Medicine, in accordance with the Guide for the care and use of laboratory animals by the United States PHS.

Genotyping

Crude genomic DNA was prepared by tissue digestion with tail buffer of 50 mM NaCl, 10 mM Tris-HCl pH.9, 0.4% NP-40, 0.4% Tween-20 and Proteinase K (New England Biolabs) for 1 h at 55°C followed by incubation at 95°C for 12 min. Samples were centrifuged at 5000 rpm for 12

min and diluted in tail buffer. Oligonucleotides used for amplification were oligo.1 - Fw GTGGTTAGCTAAAGTGAGGATGAT and oligo.2 - Rv GTGGGCTCTATGGCTTCTGAGG for the *Fmr1*^{KO} allele and oligo.1 with oligo.3 - Rv CAGGTTTGTTGGGATTAACAGATC for the WT allele, respectively (annealing at 56°C for WT and 60°C for *Fmr1*^{KO}, extension at 68°C for WT and 72°C for *Fmr1*^{KO}, cycled 35 times).

Primary hippocampal cultures

Primary cultures for WT and *Fmr1*^{KO} Ca^{2+} imaging were prepared from P0/P1 pups generated by crossing *Fmr1* heterozygous females with WT males. The dissected brains were stored in the dark at 4°C in Hibernate medium (Gibco) until genotype determination (see Genotyping). Hippocampi were microdissected in $Ca^{2+/}Mg^{2+}$-free HBSS, finely chopped and incubated for 30 min at 37°C with 1 mg/ml papain (Worthington), 1 mM $CaCl_2$, 0.5 mM EDTA, 3 mM NaOH, 0.2 mg/mL cysteine in adult HBS solution of (in mM) 145 NaCl, 22 KCl, 5 glucose, 10 HEPES, pH 7.3 supplemented with 50 µl/mL DNAse. After removing the papain, the tissue was washed with HBS and triturated in plating medium made of MEM, 10% fetal bovine serum, 2 mM GlutaMax by pipetting 15-20 times (three rounds at 3 min intervals). The dissociated cells were centrifuged at 1100 rpm for 5 min and the pellet suspended in plating medium to count viable cells using trypan blue dye exclusion. For Ca^{2+} imaging, 60,000 to 90,000 cells were plated onto 35 mm dishes with glass bottom (14 mm diameter, No. 0; MatTek Life Sci.) coated with poly-L-lysine (Sigma Aldrich) and incubated for 1 h at 37°C before removing the plating medium and replacing with growth medium made of Neurobasal-A without phenol red supplemented with 2 mM GlutaMax (both from Gibco) and 2% NeuroCult SM1 Supplement (STEMCELL Tech.). For immunofluorescence, 70,000 cells were plated onto poly-L-lysine-coated glass covers (12 mm

diameter, No. 1) in 24-well plates and incubated in plating medium for 1 h before replacing the medium as above. At d.i.v. 2, a mix of 37 mM uridine and 27 mM 5-fluoro-2-deoxyuridine (Sigma Aldrich) was added to the cultures.

Calcium imaging

To measure changes in intracellular we used the ratiometric Ca^{2+} indicator Fura-2 AM. To load cells, a stock solution (1 mM in DMSO) of membrane-permeant acetoxymethyl ester Fura-2 AM (Life Technologies, Eugene OR) was prepared and diluted to 8 µM in 1 ml of fresh growth medium (see Primary hippocampal cultures). This solution was added 1:1 (4 µM final concentration) to cells in growth medium plated onto 35 mm dishes with manually gridded glass bottom. After a 1 h incubation at 37°C, the medium was removed and the cells washed twice with modified Krebs buffer made of (in mM) 140 NaCl, 5 KCl, 2 CsCl, 5 HEPES, 5 Glucose, 2 Na-Pyruvate, 1 $MgCl_2$, 2 CaCl2, pH 7.4. After washing, cells were incubated with 1 mL of fresh modified Krebs for 15 min at 37°C before transferring to an imaging platform, Model QE-1 Quick Exchange Platform (Warner Instruments, Holliston MA) chamber with inflow and outflow tubes mounted on an Olympus IX70 (Olympus, Center Valley, PA) inverted microscope equipped with 40X UAPO340 (1.35 N.A.) and 20X UPlanAPO (0.7 N.A.) objectives. Perfusion rates were controlled using a PPS6 Peristaltic Pump Perfusion System (Warner Instruments, Holliston MA). For each imaging session, cells were superfused (2 ml/min) with modified Krebs buffer containing 0.5 µM tetrodotoxin (TTX; HelloBio) and 1 µM atropine to capture baseline Ca^{2+}, followed by co-application for 30 sec of 100 nM PNU-282987, 3 µM PNU-120596 (Cayman Chemical), 0.5 µM TTX, 1 µM atropine in modified Krebs and wash with modified Krebs containing 0.5 µM TTX, 1 µM atropine for 12-13 min during which time Ca^{2+} returned to

baseline. Ca^{2+}imaging was accomplished using a Lambda DG-4, (Sutter Instruments, Inc) illumination system that allowed rapid switching between 340 nm and 380 nm excitation wavelengths. Emission was monitored at 510 nm. Images were acquired using MetaFluor software, ver. 7.8.13, 64-bit (Molecular Devices, San Jose, CA) and an ORCA digital CMOS camera (Hamamatsu Photonics, Japan). After each session, cells were fixed with 4% paraformaldehyde (PFA) in phosphate buffered saline (PBS) for 10 min at RT and washed three times for 5 min with PBS.

F340/F380 ratiometric Ca^{2+} data exported to Excel were analyzed with OriginPro (OriginLab). F340/380 values for each cell were opened in OriginPro to build response traces; for each trace, the baseline was subtracted by manual correction using two or more points. Baseline subtracted data were graphed and batch-analyzed (5 cells/batch) with the Batch Peak Analysis tool to integrate the area under the curve of the traces for the duration of the response and identify maximum peaks. To compare the duration of the responses between different groups, the Batch Peak Analysis tool was used to integrate the area under the curve of the traces only in the first 100 sec of the response. This value was used to derive a Response Decline Index = Integrated Area first 100 sec/Integrated Area of the entire response. For rapidly declining responses, e.g. within 100 sec, the Decline Index is = 1 whereas for protracted responses (lasting >100 sec) the Decline Index is < 1. Individual traces were matched to cell neurochemical identity determined by post-hoc immunolabeling for GAD65 or GABA.

Immunofluorescence

For post-hoc immunolabeling after Ca^{2+} imaging, PFA fixed neurons in glass bottom dishes were transferred to a humidified chamber protected from light. Cells were permeabilized with 0.02% Triton X-100, 3% bovine serum albumin (BSA) in PBS for 10 min at room temperature (RT) and incubated for 1 h at RT in blocking solution of 3% BSA in PBS. Primary antibodies diluted in 1% BSA in PBS were applied for 1 h at RT followed by 3 washes with PBS for 5 min. Secondary antibodies diluted in 1% BSA in PBS were applied for 1 h at RT followed by 3 washes with PBS for 5 min. ProLong hard set antifade (Cell Signaling Technology) was added to the glass bottom of the dish and a coverslip placed on top, sandwiching the cells. For immunolabeling of surface Ly6H, 4% PFA fixed cells plated on glass bottom dishes or coverslips were directly incubated with blocking solution followed by incubation for ~ 16 h at 4ºC with anti-Ly6H diluted in 1% BSA in PBS. After washing three times with PBS, cells were incubated with permeabilization solution for 10 min and blocking solution for 1 hr at RT. Primary antibodies for MAP2 diluted in 1% BSA in PBS were added and incubated for 1 h at RT followed by three washes for 5 min with PBS. Incubation with secondary antibodies and mounting with ProLong antifade containing DAPI (Cell Signaling Technology) were as above. For hippocampal tissue labeling, mouse brains were fixed with 4% PFA for ~16 h at 4°C and washed with PBS five times for 10 min before embedding in an agarose/sucrose solution (3% agarose, 7% sucrose (w/v) in PBS). Thirty μm-thick coronal sections were cut with a vibratome (Leica Biosystems VT1000S). Floating slices were permeabilized with 0.02% TritonX-100 in PBS for 15 min and washed with PBS four times for 5 min. To quench endogenous lipofuscin, the slices were incubated with TrueBlack (Biotium) diluted 1:20 in 70% ethanol for 45 sec; the reagent was immediately removed and rapidly rinsed with PBS. The slices were washed four times with PBS and blocked with Duolink Blocking Solution (Millipore Sigma) for 30 min at RT

and incubated for ~16 h at 4ºC with anti-Ly6H and anti-MAP2 diluted in Duolink Antibody Solution (Millipore Sigma). The slices were washed four times for 5 min with PBS and incubated for 30 min at RT with donkey anti-mouse conjugated to Cy3 and donkey anti-chicken conjugated to Alexa Fluor 647 in 10% normal donkey serum in PBS. After washing four times for 5 min with PBS, the slices were mounted on glass slides with ProLong containing DAPI.

α7 nAChR labeling with α-bungarotoxin

Neurons plated on coverslips were incubated for 1 h at RT with blocking solution of 3% BSA in PBS and incubated for ~ 16 h at 4ºC with α-bungarotoxin-488 (BGTX-488; Biotium) diluted 1/500 in 1% BSA in PBS. Cells were washed with PBS three times for 5 min and permeabilized with 0.02% Triton X-100, 3% BSA in PBS for 10 min followed by incubation with blocking solution for 1 h. Anti-MAP2 antibody diluted in 1% BSA in PBS was added for 1 h at RT followed by three 5 min washes with PBS and incubation with Cy5-conjugated secondary antibody for 1 h at RT. Neurons were washed three times for 5 min with PBS and mounted with ProLong containing DAPI.

Microscopy and analysis of fluorescence

Confocal microscopy was carried out with Carl Zeiss LSM880 Airyscan using a Plan-Apochromat 63× (N.A. = 1.4) oil immersion objective. Images at 1024×1024 pixel resolution were acquired with scan speed set at 8 and pinhole configured to 1 Airy unit for each channel. Image stacks acquired with a 0.5 μm *Z* step were processed and analyzed with Fiji. For quantitative analysis of Ly6H fluorescence in primary neurons, *Z*-stacks were reconstructed using maximum intensity projection and the background subtracted from all images thresholded

to a set value of 17. Images were merged with matched DAPI/MAP2 *Z*-stacks and converted to RGB. MAP2 brightness was increased to better visualize processes and soma. A region of interest (ROI) around the soma area was outlined over the MAP2 image using the segmented line tool and saved. The Analyze Particle function (size=0.01) was used to measure Ly6H puncta area in the soma ROI and normalized to soma area. Primary dendrites connected to the soma were selected with the segmented line tool in Fiji, straightened (Line Width = 93) and segmented into 10 μm sections. To analyze Ly6H puncta within each segment, the Ly6H images were set to a fixed threshold as for the soma and converted to mask, and MAP2 images automatically thresholded with Li. The matched processed images were overlayed and Ly6H puncta area measured in each segment with the Analyze Particle tool and normalized to MAP2 area. For quantification of α-bungarotoxin labeling, BGTX-488 puncta were manually counted and normalized to the area of cell defined by MAP2 immunolabeling. Images from hippocampal slices were acquired with a Leica SP5 point-scan confocal microscope mounted with a 63x oil immersion objective (N.A. = 1.4) at 1912×1912 at pixel resolution using a scan speed set at 7, averaging of 4, and pinhole configured to 1 Airy unit for each channel. Stacks of images were acquired with a 0.6 μm Z step. For quantification with Fiji, Z stack maximum projections were background subtracted and thresholded with MaxEntropy. A region of interest (ROI) of fixed dimensions 20 x 40 μm was used to sample multiple areas of CA1 pyramidal layer and *radiatum* for each image. Epifluorescence imaging was carried out using a 20× (N.A. = 1.3) dry objective or a 60x (N.A. = 1.35) oil immersion objective mounted on a motorized Olympus IX81 inverted microscope equipped with CCD ORCA-R2 camera (Hamamatsu). Epifluorescence was used to image post-hoc labeled neurons plated on 35 mm glass bottom dishes and neurons plated on glass coverslips for BGTX-488 labeling.

Biotinylation of hippocampal slices

Hippocampi were dissected from P7-8 pups, transferred to cold Hibernate A medium (Gibco) and kept on ice. Tissue sections 400 µm-thick were prepared with a tissue chopper (McIlwain), transferred to cold External solution of (in mM) 145 NaCl, 2.5 KCl, 2 $CaCl_2$ 10 glucose, 10 Hepes (pH 7.4) on ice and separated into floating slices. For each mouse, slices from both hippocampi were washed two times with cold External solution and incubated on ice for 30 min with 1 mg/ml Sulfo-NHS-LC-biotin (Pierce and Tocris) in External solution and slowly rocked. The biotin solution was removed, and the slices washed two times with 20 mM Tris in External Solution (pH 7.5). All liquid was removed and tissue flash-frozen and stored at -80°C until use. The tissue was manually homogenized (tissue grinder 10 times; pipetting 10 times, 2 rounds) in modified RIPA buffer of 150 mM NaCl, 2 mM EDTA, 1% Triton X-100, 0.5% Na deoxycholate, 0.1% SDS, 0.1% SDS, 50 mM Tris-HCl pH 7.4 with protease inhibitors (Pierce) and centrifuged at 21,000 x *g* at 4°C for 20 min. Protein content in the supernatant was quantified by Bradford assay (Bio-Rad Labs) and equal amounts of protein per mouse mixed with 80 µl of Streptavidin-agarose resin (ThermoScientific) and incubated with end -over-end rotation for 2 h at 4°C. The resin was washed once with lysis buffer, 2 times with 0.5% Triton X-100 in phosphate buffer (PB) and 2 times with PB, with centrifugation at 500 x g for 3 min at 4°C between washes. Bound proteins were eluted in SDS-PAGE sample buffer with 100 mM DTT and heated at 95°C for 5 min along with total input proteins.

Western blot of tissue and neuron extracts

For tissue extracts, the dissected mouse hippocampus was homogenized with mechanical tissue homogenizer in lysis buffer of 50 mM Tris-HCl pH 7.4, 150 mM NaCl, 1 mM EDTA, 1% Triton

X-100, 0.5% CHAPS with protease inhibitor cocktail. Homogenates were centrifuged at 800 x *g* for 10 min at 4°C and the supernatant (S1) collected and centrifuged at 10,000 x *g* for 15 min. The resulting pellet (P2) and supernatant (S2) were separated and P2 resuspended in lysis buffer. To prepare cell extracts, hippocampal neurons from P0/P1 WT and *Fmr1*^{KO} pups from WT or *Fmr1*^{KO} crossings, respectively, were prepared as described (see Primary cultures) but plated in 24-multiwell plates coated with poly-L-lysine at 200,000 cells/well. The plating medium was completely removed after 1 h at 37°C and replaced with growth medium supplemented with uridine/-fluoro-2-deoxyuridine. Half of the media was removed and replaced with fresh growth medium in experiments in which cells were used after 7 days in vitro. Protein extracts were prepared in modified RIPA buffer and equal amounts of proteins separated by SDS-PAGE. For Western blot, proteins were transferred onto nitrocellulose membranes (0.2 µm pore size; Bio-Rad Labs) according to standard procedures. Blocking buffer contained 5% BSA when probing for Ly6H and pan-actin and 5% dry milk for α7 nAChR and tubulin. Detection was done with HRP-conjugated secondary antibodies and chemiluminescence (Immobilon; MilliporeSigma) using an Azure c600 imaging system (Azure Biosystems).

Adenovirus production and transduction

Plasmids encoding H1-pTrip-EF1a-eGFP Ly6H shRNA and H1-pTrip-EF1a-eGFP scrambled control shRNA in pAd/PL-DEST vector were a generous gift from Dr. William J. Joiner (UC San Diego, CA, USA). Plasmids were linearized by digestion with Pac I, purified and transfected with Lipofectamine 3000 (Invitrogen) according to the manufacturer's protocol in 293A cells plated in 6-well dish at 1.5 x 10^6 cells/well. Cells were maintained for10-14 days in I-MEM containing 10% fetal bovine serum, 2 mM glutamine, 10 mM Hepes, 100 U/ml penicillin, 100

μg/ml streptomycin. After collecting the supernatant, cells suspended in PBS were disrupted with three rounds of freeze-thaw and spun down. The combined supernatants (1/7 of total) were used to infect 293A cells plated onto 100 mm dishes that were harvested 4-6 days to repeat the amplification (1-2 times). The concentration of viral particles in PBS was determined by measuring absorbance at 260 nm (OD_{260}) to calculate optical viral particle (OVP)/ml: OD_{260} x 0.005 (dilution factor) x 1.1×10^{12} OVP. Viral particles were aliquoted, flash frozen and stored at -80°C until use. For knockdown, neurons from P0/1 pups derived from *Fmr1*^{KO} crossings were transduced at d.i.v. 2 with viral particles at multiplicity of infection (M.O.I.) 20-30:1 calculated from initial plating density. Briefly, after removing about one third of medium (conditioned medium) from the 35 mm dishes in which neurons were plated, viral particles diluted in 100 μl fresh growth medium (see Primary hippocampal cultures) were added to the dishes and incubated for 8 h at 37°C. The medium was then completely replaced with a mixture of conditioned medium and fresh growth medium containing uridine/5-fluoro-2-deoxyuridine. Neurons were maintained in culture for 7 days until analysis at d.i.v. 9.

In vivo delivery of PNU-120596

Mice were weighed at P17 to determine dose/volume of PNU-120596 for intraperitoneal (i.p.) injection calculated from the average weight of the litter according to the formula V_{inj}= ([D] x m_{mouse})/C_1, where V_{inj} is the injection volume, D is the final concentration of drug in the animal, m_{mouse} is the average weight of the litter in kg, and C_1 is the working concentration of PNU-120596 injected. The working concentration was calculated to ensure that no more than ~10 μl/g body weight was injected. PNU-120596 (Cayman Chemical) was dissolved in DMSO to make a stock of 100 mM (31.172 mg/ml): on the day of the injection, the stock solution was diluted to a

working concentration of 0.3 mg/ml in a solution of 10% DMSO, 90% corn oil (Sigma Life Sciences) filter-sterilized. The vehicle solution contained 10% DMSO, 90% corn oil. PNU-120596 or vehicle was back filled into a 1 mL syringe (Slip Tip with Intradermal Bevel Needle, 26G x 3/8; BD Syringe) and delivered daily by i.p. injection from P18 to P22, alternating the side the solution was injected each day. Injections were performed blind to treatment condition. After completion of data acquisition and analysis, the respective treatment conditions were identified based on marks in the mouse tail made at P7. Male and female mice from *Fmr1*^{KO} crossings were used for drug treatment for behavioral studies.

Hyperactivity

Drug-treated mice at age P22 were transferred from the animal facility and allowed to habituate to the laboratory room for > 30 min. All litters were tested starting around 4 PM to minimize possible circadian effects and the procedure carried out in a dedicated, isolated room. The testing chamber was housed inside a Styrofoam box with a hole on the top allowing placement of a camera to record videos from above. Once a mouse was placed inside the testing chamber a glass lid was installed on top of the chamber. Mice were tracked for a total of 10 min including during the first 5 min of habituation to the chamber and 5 min for observation of activity. Mouse behavior was analyzed with EthoVision software (Noldus) and total distance traveled, frequency of movement initiation and movement duration (% of total time) were measured.

Audiogenic seizures

Immediately after recording motor activity, the susceptibility and severity of audiogenic seizures was tested utilizing an alarm (Portable Safety Kit Door Alarm; RadioShack) positioned to the

right and above the testing chamber. To elicit seizures, the alarm set at ~120 dB was turned on for 60 sec and the seizure behavior videorecorded. Audiogenic seizures were scored using a Audiogenic Response Score (ARS) according to Jobe et. al (*67*) that was specifically designed to capture the signs and severity of these generalized motor seizures. The ARS values from 1 to 9, in increasing order of severity, included ARS 1, one bout of wild run (WR1); ARS 2, two bouts of wild run (WR2) and generalized clonus; ARS 3, one bout of wild run (WR1) and generalized clonus; ARS 4, WR2 and tonic flexion of neck, trunk, and forelimbs with clonus of hindlimbs; ARS 5, WR1 and tonic flexion of neck, trunk, and forelimbs with clonus of hindlimbs; ARS 6, WR2 and tonic flexion of neck, trunk, and forelimbs with hindlimb partial tonic extension; ARS 7, WR1 and tonic flexion of neck, trunk, and forelimbs with hindlimb partial tonic extension; ARS 8, WR2 and tonic flexion of neck, trunk, and forelimbs with hindlimb complete tonic extension; ARS 9, WR1 + tonic flexion of neck, trunk, and forelimbs with hindlimb complete tonic extension.

Antibodies

Mouse anti-Ly6H, Abnova # H00004062-M01, AB_425531; IF 1:400; WB 1:1000.

Mouse anti-GAD65, DSHB GAD-6; AB_2314499; IF 1:400.

Mouse anti-γ-Tubulin, Sigma Aldrich GTU-88, AB_477584; WB 1:2500.

Rabbit anti-pan actin, Cell Signaling Technology AB_10998774; WB 1:1000.

Rabbit polyclonal anti-α7 nAChR, Alomone Labs, AB_10659339; WB 1:500 .

Rabbit polyclonal anti-GABA, Sigma Aldrich, AB_477652; IF 1/8000.

Chicken anti-MAP2, PhosphoSolutions, AB_2492141; IF 1:500 (cells) or 1:400 (slices).

The following secondary antibodies were used according to manufacturer's specification: donkey anti-mouse and anti-rabbit conjugated to AlexaFluor-488, -647 (Invitrogen), Cy3 (Jackson ImmunoResearch Labs), anti-chicken conjugated to AlexaFluor-647, aminomethylcoumarin acetate (Jackson ImmunoResearch Labs), goat anti-mouse and rabbit conjugated to horseradish peroxidase (Jackson ImmunoResearch Labs).

Statistical analysis

Data were analyzed by GraphPad Prism 8.1 software. Unless otherwise indicated, statistical significance was determined by t test (two-tailed) or one-way analysis of variance (ANOVA) (Tukey's multiple-comparison post test), with $p < 0.05$ considered significant.

Supplementary Materials

Fig. S1. Ly6H protein expression during hippocampal early postnatal development.

Fig. S2. The total abundance of Ly6H is not altered in *Fmr1*^{KO} hippocampal neurons.

Fig. S3. α7 subunit expression is not altered in *Fmr1*^{KO} mice.

Fig. S4. Expression of BGTX-labeled mature α7 nAChRs is not altered in *Fmr1*^{KO} GABAergic cells.

Fig. S5. Reduced expression of Ly6H in neurons transduced with Ly6H shRNA.

Fig. S6. Audiogenic Seizure Response Score.

References

1. J. Hunter, O. Rivero-Arias, A. Angelov, E. Kim, I. Fotheringham, J. Leal, Epidemiology of fragile X syndrome: A systematic review and meta-analysis. *American Journal of Medical Genetics Part A* **164**, 1648-1658 (2014).
2. D. B. Bailey Jr, M. Raspa, M. Olmsted, D. B. Holiday, Co-occurring conditions associated with FMR1 gene variations: Findings from a national parent survey. *American Journal of Medical Genetics Part A* **146**, 2060-2069 (2008).
3. W. E. Kaufmann, S. A. Kidd, H. F. Andrews, D. B. Budimirovic, A. Esler, B. Haas-Givler, T. Stackhouse, C. Riley, G. Peacock, S. L. Sherman, W. T. Brown, E. Berry-Kravis, Autism spectrum disorder in fragile X syndrome: cooccurring conditions and current treatment. *Pediatrics* **139**, S194-S206 (2017).
4. A. J. Verkerk, M. Pieretti, J. S. Sutcliffe, Y.-H. Fu, D. P. Kuhl, A. Pizzuti, O. Reiner, S. Richards, M. F. Victoria, F. Zhang, Identification of a gene (FMR-1) containing a CGG repeat coincident with a breakpoint cluster region exhibiting length variation in fragile X syndrome. *Cell* **65**, 905-914 (1991).
5. J. D. Richter, X. Zhao, The molecular biology of FMRP: new insights into fragile X syndrome. *Nature Reviews Neuroscience* **22**, 209-222 (2021).

6. X. Liu, V. Kumar, N.-P. Tsai, B. D. Auerbach, Hyperexcitability and homeostasis in fragile X syndrome. *Frontiers in Molecular Neuroscience* **14**, 805929 (2022).
7. L. M. Teles-Grilo Ruivo, J. R. Mellor, Cholinergic modulation of hippocampal network function. *Frontiers in Synaptic Neuroscience* **5**, (2013).
8. L. Maggi, E. Sher, E. Cherubini, Regulation of GABA release by nicotinic acetylcholine receptors in the neonatal rat hippocampus. *The Journal of Physiology* **536**, 89-100 (2001).
9. J. L. Yakel, Nicotinic ACh receptors in the hippocampal circuit; functional expression and role in synaptic plasticity. *The Journal of Physiology* **592**, 4147-4153 (2014).
10. H. Lin, F.-C. Hsu, B. H. Baumann, D. A. Coulter, S. A. Anderson, D. R. Lynch, Cortical parvalbumin GABAergic deficits with α7 nicotinic acetylcholine receptor deletion: implications for schizophrenia. *Molecular and Cellular Neuroscience* **61**, 163-175 (2014).
11. A. F. Lozada, X. Wang, N. V. Gounko, K. A. Massey, J. Duan, Z. Liu, D. K. Berg, Glutamatergic synapse formation is promoted by α7-containing nicotinic acetylcholine receptors. *Journal of Neuroscience* **32**, 7651-7661 (2012).
12. Z. Liu, R. A. Neff, D. K. Berg, Sequential interplay of nicotinic and GABAergic signaling guides neuronal development. *Science* **314**, 1610-1613 (2006).
13. S. R. Thomson, S. S. Seo, S. A. Barnes, S. R. Louros, M. Muscas, O. Dando, C. Kirby, D. J. Wyllie, G. E. Hardingham, P. C. Kind, E. K. Osterweil, Cell-type-specific translation profiling reveals a novel strategy for treating fragile X syndrome. *Neuron* **95**, 550-563.e555 (2017).

14. L. J. Volk, B. E. Pfeiffer, J. R. Gibson, K. M. Huber, Multiple Gq-coupled receptors converge on a common protein synthesis-dependent long-term depression that is affected in fragile X syndrome mental retardation. *Journal of Neuroscience* **27**, 11624-11634 (2007).

15. M. A. Gillentine, C. P. Schaaf, The human clinical phenotypes of altered CHRNA7 copy number. *Biochemical Pharmacology* **97**, 352-362 (2015).

16. J. W. Young, N. Crawford, J. S. Kelly, L. E. Kerr, H. M. Marston, C. Spratt, K. Finlayson, J. Sharkey, Impaired attention is central to the cognitive deficits observed in alpha 7 deficient mice. *European Neuropsychopharmacology* **17**, 145-155 (2007).

17. J. A. Matta, S. Gu, W. B. Davini, B. Lord, E. R. Siuda, A. W. Harrington, D. S. Bredt, NACHO mediates nicotinic acetylcholine receptor function throughout the brain. *Cell Reports* **19**, 688-696 (2017).

18. A. J. Sharp, H. C. Mefford, K. Li, C. Baker, C. Skinner, R. E. Stevenson, R. J. Schroer, F. Novara, M. De Gregori, R. Ciccone, A. Broomer, I. Casuga, Y. Wang, C. Xiao, C. Barbacioru, G. Gimelli, B. D. Bernardina, C. Torniero, R. Giorda, R. Regan, V. Murday, S. Mansour, M. Fishera, L. Castiglia, P. Failla, M. Ventura, Z. Jiang, G. M. Cooper, S. J. Knight, C. Romano, O. Zuffardi, C. Chen, C. E. Schwartz, E. E. Eichler, A recurrent 15q13.3 microdeletion syndrome associated with mental retardation and seizures. *Nature Genetics* **40**, 322 (2008).

19. C. E. Adams, J. C. Yonchek, K. M. Schulz, S. L. Graw, J. Stitzel, P. U. Teschke, K. E. Stevens, Reduced Chrna7 expression in mice is associated with decreases in hippocampal markers of inhibitory function: implications for neuropsychiatric diseases. *Neuroscience* **207**, 274-282 (2012).

20. R. S. Hurst, M. Hajos, M. Raggenbass, T. M. Wall, N. R. Higdon, J. A. Lawson, K. L. Rutherford-Root, M. B. Berkenpas, W. E. Hoffmann, D. W. Piotrowski, V. E. Groppi, G. Allaman, R. Ogier, S. Bertrand, D. Bertrand, S. P. Arneric, A novel positive allosteric modulator of the α7 neuronal nicotinic acetylcholine receptor: in vitro and in vivo characterization. *Journal of Neuroscience* **25**, 4396-4405 (2005).
21. S. Fucile, Ca2+ permeability of nicotinic acetylcholine receptors. *Cell Calcium* **35**, 1-8 (2004).
22. S. F. Colombo, F. Mazzo, F. Pistillo, C. Gotti, Biogenesis, trafficking and up-regulation of nicotinic ACh receptors. *Biochemical Pharmacology* **86**, 1063-1073 (2013).
23. J. M. Miwa, K. R. Anderson, K. M. Hoffman, Lynx prototoxins: Roles of endogenous mammalian neurotoxin-like proteins in modulating nicotinic acetylcholine receptor function to influence complex biological processes. *Frontiers in Pharmacology* **10**, 343 (2019).
24. I. Ibañez-Tallon, J. M. Miwa, H.-L. Wang, N. C. Adams, G. W. Crabtree, S. M. Sine, N. Heintz, Novel Modulation of Neuronal Nicotinic Acetylcholine Receptors by Association with the Endogenous Prototoxin lynx1. *Neuron* **33**, 893-903 (2002).
25. C. A. Puddifoot, M. L. Wu, R. J. Sung, W. J. Joiner, Ly6h Regulates Trafficking of Alpha7 Nicotinic Acetylcholine Receptors and Nicotine-Induced Potentiation of Glutamatergic Signaling. *Journal of Neuroscience* **35**, 3420-3430 (2015).
26. M. L. Wu, C. A. Puddifoot, P. Taylor, W. J. Joiner, Mechanisms of Inhibition and Potentiation of alpha 4132 Nicotinic Acetylcholine Receptors by Members of the Ly6 Protein Family. *Journal of Biological Chemistry* **290**, 24509-24518 (2015).

27. M. Kalinowska, C. Castillo, A. Francesconi, Quantitative profiling of brain lipid raft proteome in a mouse model of fragile X syndrome. *PloS One* **10**, e0121464 (2015).

28. M. L. Wu, C. Z. Liu, E. A. Barrall, R. A. Rissman, W. J. Joiner, Unbalanced regulation of α7 nAChRs by Ly6h and NACHO contributes to neurotoxicity in Alzheimer's disease. *Journal of Neuroscience* **41**, 8461-8474 (2021).

29. Y. Moriwaki, N. Kubo, M. Watanabe, S. Asano, T. Shinoda, T. Sugino, D. Ichikawa, S. Tsuji, F. Kato, H. Misawa, Endogenous neurotoxin-like protein Ly6H inhibits alpha7 nicotinic acetylcholine receptor currents at the plasma membrane. *Scientific Reports* **10**, 11996 (2020).

30. M. S. Cembrowski, J. L. Bachman, L. Wang, K. Sugino, B. C. Shields, N. Spruston, Spatial gene-expression gradients underlie prominent heterogeneity of CA1 pyramidal neurons. *Neuron* **89**, 351-368 (2016).

31. M. Karlsson, C. Zhang, L. Méar, W. Zhong, A. Digre, B. Katona, E. Sjöstedt, L. Butler, J. Odeberg, P. Dusart, F. Edfors, P. Oksvold, K. von Feilitzen, M. Zwahlen, M. Arif, O. Altay, X. Li, M. Ozcan, A. Mardinoglu, L. Fagerberg, J. Mulder, Y. Luo, F. Ponten, M. Uhlen, C. Lindskog, A single–cell type transcriptomics map of human tissues. *Science Advances* **7**, eabh2169 (2021).

32. F. Pontén, K. Jirström, M. Uhlen, The Human Protein Atlas—a tool for pathology. *The Journal of Pathology: A Journal of the Pathological Society of Great Britain and Ireland* **216**, 387-393 (2008).

33. M. S. Thomsen, B. Cinar, M. M. Jensen, E. N. Lyukmanova, M. A. Shulepko, V. Tsetlin, A. B. Klein, J. D. Mikkelsen, Expression of the Ly-6 family proteins Lynx1 and Ly6H in

the rat brain is compartmentalized, cell-type specific, and developmentally regulated. *Brain Structure & Function* **219**, 1923-1934 (2014).

34. M. Alkondon, E. X. Albuquerque, Diversity of nicotinic acetylcholine receptors in rat hippocampal neurons. I. Pharmacological and functional evidence for distinct structural subtypes. *Journal of Pharmacology and Experimental Therapeutics* **265**, 1455-1473 (1993).
35. R. Freedman, C. Wetmore, I. Stromberg, S. Leonard, L. Olson, Alpha-bungarotoxin binding to hippocampal interneurons: immunocytochemical characterization and effects on growth factor expression. *Journal of Neuroscience* **13**, 1965-1975 (1993).
36. C. E. Adams, R. S. Broide, Y. Chen, U. H. Winzer-Serhan, T. A. Henderson, F. M. Leslie, R. Freedman, Development of the α7 nicotinic cholinergic receptor in rat hippocampal formation. *Developmental Brain Research* **139**, 175-187 (2002).
37. M. Hajos, R. Hurst, W. Hoffmann, M. Krause, T. M. Wall, N. R. Higdon, V. E. Groppi, The selective α7 nicotinic acetylcholine receptor agonist PNU-282987 [N-[(3R)-1-azabicyclo [2.2. 2] oct-3-yl]-4-chlorobenzamide hydrochloride] enhances GABAergic synaptic activity in brain slices and restores auditory gating deficits in anesthetized rats. *Journal of Pharmacology and Experimental Therapeutics* **312**, 1213-1222 (2005).
38. Z. Gu, K. G. Smith, G. M. Alexander, I. Guerreiro, S. M. Dudek, B. Gutkin, P. Jensen, J. L. Yakel, Hippocampal interneuronal α7 nAChRs modulate theta oscillations in freely moving mice. *Cell Reports* **31**, (2020).
39. K. Ganguly, A. F. Schinder, S. T. Wong, M.-m. Poo, GABA itself promotes the developmental switch of neuronal GABAergic responses from excitation to inhibition. *Cell* **105**, 521-532 (2001).

40. R. Tyzio, G. L. Holmes, Y. Ben-Ari, R. Khazipov, Timing of the developmental switch in GABAA mediated signaling from excitation to inhibition in CA3 rat hippocampus using gramicidin perforated patch and extracellular recordings. *Epilepsia* **48**, 96-105 (2007).

41. Q. Yan, M. Rammal, M. Tranfaglia, R. P. Bauchwitz, Suppression of two major Fragile X Syndrome mouse model phenotypes by the mGluR5 antagonist MPEP. *Neuropharmacology* **49**, 1053-1066 (2005).

42. T. M. Kazdoba, P. T. Leach, J. L. Silverman, J. N. Crawley, Modeling fragile X syndrome in the Fmr1 knockout mouse. *Intractable & Rare Diseases Research* **3**, 118-133 (2014).

43. Y. Zhang, S.-X. Cao, P. Sun, H.-Y. He, C.-H. Yang, X.-J. Chen, C.-J. Shen, X.-D. Wang, Z. Chen, D. K. Berg, S. Duan, X.-M. Li, Loss of MeCP2 in cholinergic neurons causes part of RTT-like phenotypes via α7 receptor in hippocampus. *Cell Research* **26**, 728-742 (2016).

44. N. K. Sharma, S. Kaur, R. K. Goel, Exploring the ameliorative role of α7 neuronal nicotinic acetylcholine receptor modulation in epilepsy and associated comorbidities in post-PTZ-kindled mice. *Epilepsy & Behavior* **103**, 106862 (2020).

45. P. Sun, D.-G. Liu, X.-M. Ye, Nicotinic acetylcholine receptor α7 subunit is an essential regulator of seizure susceptibility. *Frontiers in Neurology* **12**, 656752 (2021).

46. J.-J. Zheng, T.-Y. Zhang, H.-T. Liu, Z.-X. Huang, J.-M. Teng, J.-X. Deng, J.-G. Zhong, X. Qian, X.-W. Sheng, J.-Q. Ding, S.-Q. He, X. Zhao, W.-D. Ji, D.-F. Qi, W. Li, M. Zhang, Cytisine exerts an anti-epileptic effect via α7nAChRs in a rat model of temporal lobe epilepsy. *Frontiers in Pharmacology* **12**, 706225 (2021).

47. L. G. Romanova, Z. A. Zorina, L. I. Korochkin, A genetic, physiological, and biochemical investigation of audiogenic seizures in rats. *Behavior Genetics* **23**, 483-489 (1993).

48. K. C. Ross, J. R. Coleman, Developmental and genetic audiogenic seizure models: behavior and biological substrates. *Neuroscience & Biobehavioral Reviews* **24**, 639-653 (2000).

49. J. A. Matta, S. Gu, W. B. Davini, D. S. Bredt, Nicotinic acetylcholine receptor redux: Discovery of accessories opens therapeutic vistas. *Science* **373**, eabg6539 (2021).

50. T. Maurin, K. Lebrigand, S. Castagnola, A. Paquet, M. Jarjat, A. Popa, M. Grossi, F. Rage, B. Bardoni, HITS-CLIP in various brain areas reveals new targets and new modalities of RNA binding by fragile X mental retardation protein. *Nucleic Acids Research* **46**, 6344-6355 (2018).

51. J. C. Darnell, S. J. Van Driesche, C. Zhang, K. Y. S. Hung, A. Mele, C. E. Fraser, E. F. Stone, C. Chen, J. J. Fak, S. W. Chi, D. D. Licatalosi, J. D. Richter, R. B. Darnell, FMRP stalls ribosomal translocation on mRNAs linked to synaptic function and autism. *Cell* **146**, 247-261 (2011).

52. A. B. Tekinay, Y. Nong, J. M. Miwa, I. Lieberam, I. Ibanez-Tallon, P. Greengard, N. Heintz, A role for LYNX2 in anxiety-related behavior. *Proceedings of the National Academy of Sciences* **106**, 4477-4482 (2009).

53. J. M. Miwa, I. Ibañez-Tallon, G. W. Crabtree, R. Sánchez, A. Šali, L. W. Role, N. Heintz, lynx1, an endogenous toxin-like modulator of nicotinic acetylcholine receptors in the mammalian CNS. *Neuron* **23**, 105-114 (1999).

54. E. Dessaud, D. Salaün, O. Gayet, M. Chabbert, O. deLapeyriere, Identification of lynx2, a novel member of the ly-6/neurotoxin superfamily, expressed in neuronal subpopulations during mouse development. *Molecular and Cellular Neuroscience* **31**, 232-242 (2006).

55. M. J. Boland, K. L. Nazor, H. T. Tran, A. Szücs, C. L. Lynch, R. Paredes, F. Tassone, P. P. Sanna, R. J. Hagerman, J. F. Loring, Molecular analyses of neurogenic defects in a human pluripotent stem cell model of fragile X syndrome. *Brain* **140**, 582-598 (2017).

56. K. Talvio, R. Minkeviciene, K. G. Townsley, V. S. Achuta, L. M. Huckins, P. Corcoran, K. J. Brennand, M. L. Castrén, Reduced LYNX1 expression in transcriptome of human iPSC-derived neural progenitors modeling fragile X syndrome. *Frontiers in Cell and Developmental Biology* **10**, 1034679 (2022).

57. N. R. Campbell, C. C. Fernandes, A. W. Halff, D. K. Berg, Endogenous signaling through α7-containing nicotinic receptors promotes maturation and integration of adult-born neurons in the hippocampus. *Journal of Neuroscience* **30**, 8734-8744 (2010).

58. L. Maggi, C. Le Magueresse, J.-P. Changeux, E. Cherubini, Nicotine activates immature "silent" connections in the developing hippocampus. *Proceedings of the National Academy of Sciences* **100**, 2059-2064 (2003).

59. A. Tempio, A. Boulksibat, B. Bardoni, S. Delhaye, Fragile X Syndrome as an interneuronopathy: a lesson for future studies and treatments. *Frontiers in Neuroscience* **17**, 1171895 (2023).

60. R. J. Hagerman, E. Berry-Kravis, H. C. Hazlett, D. B. Bailey, H. Moine, R. F. Kooy, F. Tassone, I. Gantois, N. Sonenberg, J. L. Mandel, P. J. Hagerman, Fragile X syndrome. *Nature Reviews Disease Primers* **3**, 1-19 (2017).

61. A. P. Domanski, S. A. Booker, D. J. A. Wyllie, J. T. R. Isaac, P. C. Kind, Cellular and synaptic phenotypes lead to disrupted information processing in Fmr1-KO mouse layer 4 barrel cortex. *Nature Communications* **10**, 4814 (2019).

62. E. N. Falk, K. J. Norman, Y. Garkun, M. P. Demars, S. Im, G. Taccheri, J. Short, K. Caro, S. E. McCraney, C. Cho, M. R. Smith, H.-M. Lin, H. Koike, J. Bateh, P. Maccario, L. Waltrip, M. Janis, H. Morishita, Nicotinic regulation of local and long-range input balance drives top-down attentional circuit maturation. *Science Advances* **7**, eabe1527 (2021).

63. C. A. Trujillo, J. W. Adams, P. D. Negraes, C. Carromeu, L. Tejwani, A. Acab, B. Tsuda, C. A. Thomas, N. Sodhi, K. M. Fichter, S. Romero, F. Zanella, T. J. Sejnowski, H. Ulrich, A. R. Muotri, Pharmacological reversal of synaptic and network pathology in human MECP2-KO neurons and cortical organoids. *EMBO Molecular Medicine* **13**, e12523 (2021).

64. A. S. Lewis, G. I. van Schalkwyk, M. O. Lopez, F. R. Volkmar, M. R. Picciotto, D. G. Sukhodolsky, An exploratory trial of transdermal nicotine for aggression and irritability in adults with autism spectrum disorder. *Journal of Autism and Developmental Disorders* **48**, 2748-2757 (2018).

65. A. Contractor, V. A. Klyachko, C. Portera-Cailliau, Altered neuronal and circuit excitability in fragile X syndrome. *Neuron* **87**, 699-715 (2015).

66. K. W. Gee, A. Olincy, R. Kanner, L. Johnson, D. Hogenkamp, J. Harris, M. Tran, S. A. Edmonds, W. Sauer, R. Yoshimura, T. Johnstone, R. Freedman, First in human trial of a type I positive allosteric modulator of alpha7-nicotinic acetylcholine receptors:

Pharmacokinetics, safety, and evidence for neurocognitive effect of AVL-3288. *Journal of Psychopharmacology* **31**, 434-441 (2017).

67. P. C. Jobe, A. L. Picchioni, L. Chin, Role of brain 5-hydroxytryptamine in audiogenic seizure in the rat. *Life Sciences* **13**, 1-13 (1973).

Acknowledgments: We thank the members of the Francesconi laboratory for assistance with methodology and critical insights. We thank Noelie Cayla for assistance with EthoVision. We acknowledge the assistance of the Neural Cell Engineering and Imaging Core of the Einstein Rose F. Kennedy Intellectual and Developmental Disabilities Research Center supported by the National Institute of Child Health and Human Development U54 HD090260.

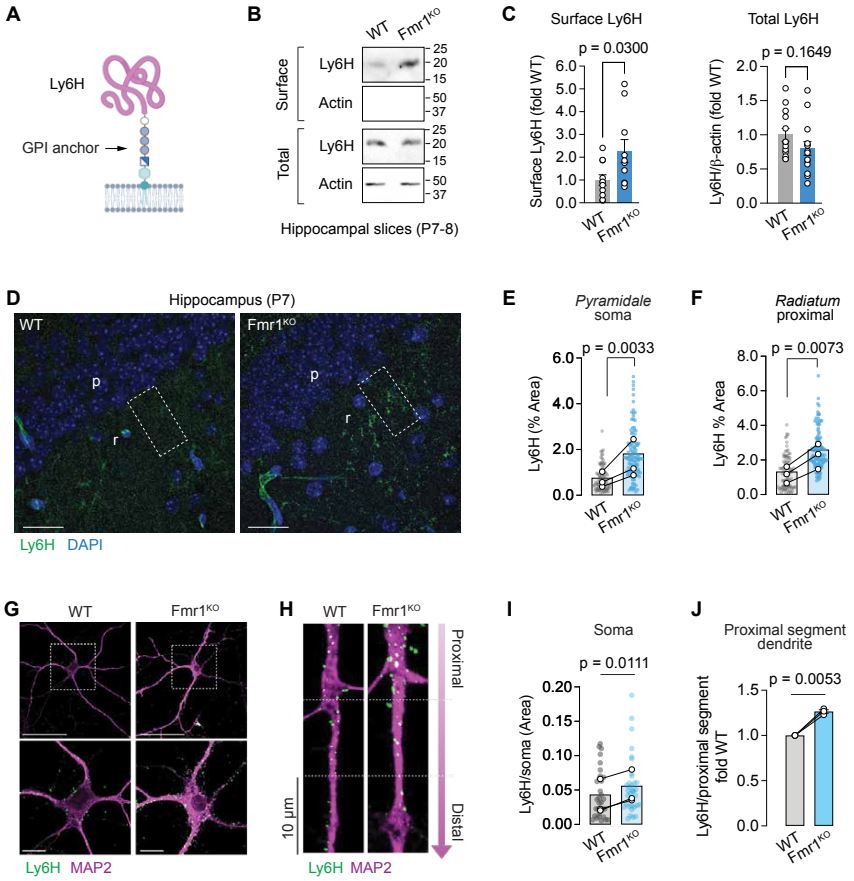

Fig. 1. Ly6H surface expression is increased in *Fmr1* KO hippocampal neurons. (A) Schematic of Ly6H protein structure (created with Biorender). (**B**) Representative Western blots of biotin-labeled (surface) and total Ly6H in hippocampal slices from WT and *Fmr1*^{KO} mice at P7-8; Actin (pan) served as loading control. (**C**) Quantification of Ly6H surface expression (left, WT n = 11 mice, *Fmr1*^{KO} n = 10) normalized to total Ly6H (right, WT n = 13, *Fmr1*^{KO} n = 14); unpaired t test. (**D**) Representative confocal images of Ly6H immunolabeling and nuclei stained with DAPI in hippocampal slices from WT and *Fmr1*^{KO} mice at P7. Shown is area CA1: *p*, pyramidal layer, *r*, *stratum radiatum*; outlined regions (20 x 40 µm) are representative of regions in the *radiatum* where Ly6H expression was quantified; scale bars, 25 µm. (**E**) Quantification of Ly6H expression in the CA1 pyramidal layer containing neuron soma; the graph illustrates the percentage of Ly6H^{+} area in 20 x 40 µm regions randomly selected in the pyramidal layer of P7 and P22 mice (N =3 mice per genotype). Filled symbols in the scatter plot correspond to all regions analyzed (WT, n = 91; *Fmr1*^{KO} n = 110). White outlined symbols correspond to mean values of matched littermates (mean ± SEM WT, 0.66 ± 0.19; *Fmr1*^{KO}, 1.5 ± 0.48), ratio paired t test. (**F**) Quantification of Ly6H in the WT and *Fmr1*^{KO} *radiatum,* harboring the apical dendrites of pyramidal neurons; the graph illustrates the percentage of Ly6H^{+} area in 20 x 40 µm regions randomly selected, as indicated in (D). Filled symbols correspond to all regions analyzed (WT, n = 94; *Fmr1*^{KO} n = 113) and white outlined symbols are the means (N =3) of matched littermates (mean ± SEM WT, 1.2 ± 0.27; *Fmr1*^{KO}, 2.2 ± 0.42); ratio paired t test. (**G**) Representative confocal images of surface Ly6H in the somatodendritic region of primary WT and *Fmr1*^{KO} hippocampal neurons at d.i.v. 7 with outlined soma proximal regions shown magnified below; scale bars 50 and 10 µm, respectively. (**H**) Representative confocal images of Ly6H surface expression in the proximal region of WT and *Fmr1*^{KO} primary dendrites. The first three proximal dendritic segments (closest to the soma) are shown, each 10 µm in length. (**I**) Quantification of somatic Ly6H^{+} puncta area normalized to soma area in WT and *Fmr1*^{KO} neurons from images as in (G). Filled symbols represent all soma analyzed (WT n = 33, *Fmr1*^{KO} n = 36), the outlined white symbols are the means from individual matched cultures (N=3, 1-2 pups/genotype); mean ± SEM WT, 0.036 ± 0.015; *Fmr1*^{KO}, 0.051 ± 0.014; paired t test. (**J**) Quantification of *Fmr1*^{KO}/WT fold difference in normalized Ly6H^{+} puncta area in the first dendritic proximal segment from images as in (H). KO/WT ratio mean ± SEM, 1.3 ± 0.019 from N=3 cultures in which in aggregate n = 137 and n = 126 proximal dendritic segments were quantified for WT and *Fmr1*^{KO}, respectively; one sample t test.

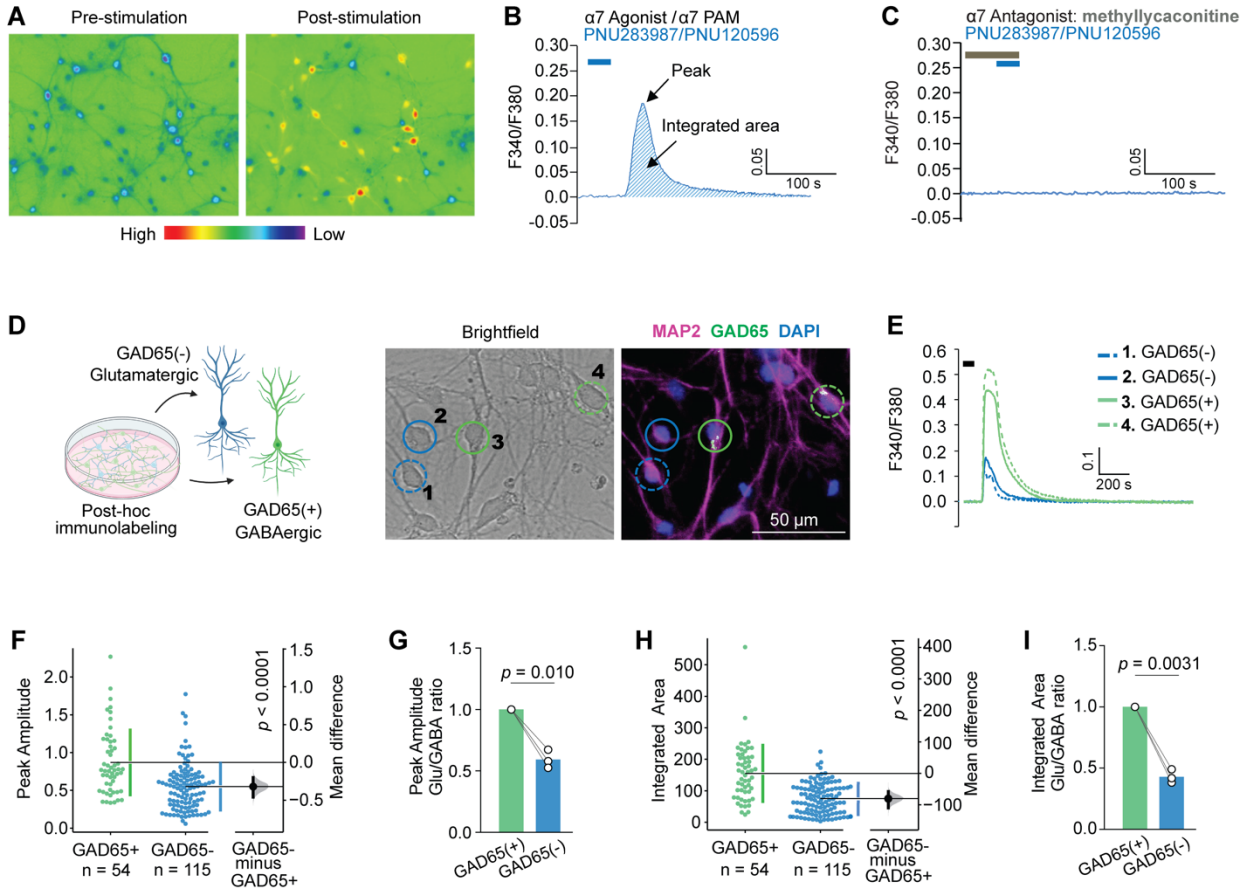

Fig. 2. Immature GABAergic cells show stronger α7 nAChR-mediated Ca^{2+} responses compared to glutamatergic neurons. (**A**) Representative images of changes in $Ca^{2+}{}_i$ detected with Fura-2 AM in WT hippocampal neurons before (pre) and after (post) stimulation with bath-applied α7 nAChR agonist (100 nM PNU-282987) together with PAM (3 µM PNU-120596); high/low heatmap visualizes $Ca^{2+}{}_i$ level. (**B**) Representative trace of an evoked α7 nAChR-mediated Ca^{2+} response in a WT hippocampal neuron (d.i.v. 9). (**C**) The $Ca^{2+}{}_1$ raise induced by stimulation with PNU-282987/PNU-120596 is blocked by the selective α7 nAChR antagonist methyllycaconitine (10 nM, MLA). (**D**) Schematic of the strategy to distinguish immature GABAergic (GAD65+) *vs*. glutamatergic (GAD65-) hippocampal neurons (left panel; created with Biorender) and representative images of d.i.v. 7 GAD65(+) (green circles) and GAD65(-) (blue circles) neurons; scale bar 50 µm. (**E**) Evoked α7 nAChR responses in the GAD65(+) and GAD65(-) cells circled in (D). (**F**) Quantification of peak amplitude of α7 nAChR responses in individual GAD65(+) and GAD65(-) neurons from N=3 independent experiments. Gardner-Altman estimation plot; group values (left axes) and mean difference (right floating axes) shown as a bootstrap sampling distribution. The mean difference is indicated by the dot and the 95% confidence interval is indicated by the error bar; two-sided permutation t test. (**G**) Relative magnitude of peak amplitude in GAD65(-) *vs.* GAD65(+) neurons expressed as ratio of mean peak amplitudes; GAD65(-)/GAD65(+) ratio mean ± SEM, 0.59 ± 0.043, N =3, one sample t test. (**H**) Quantification of response integrated area in GAD65(+) and GAD65(-) neurons from N=3 experiments; Gardner-Altman estimation plot, two-sided permutation t test. (**I**) Relative magnitude of the integrated area expressed as ratio of mean peak amplitudes; GAD65(-) /GAD65(+) ratio mean ± SEM, 0.43 ± 0.032, N =3, one sample t test.

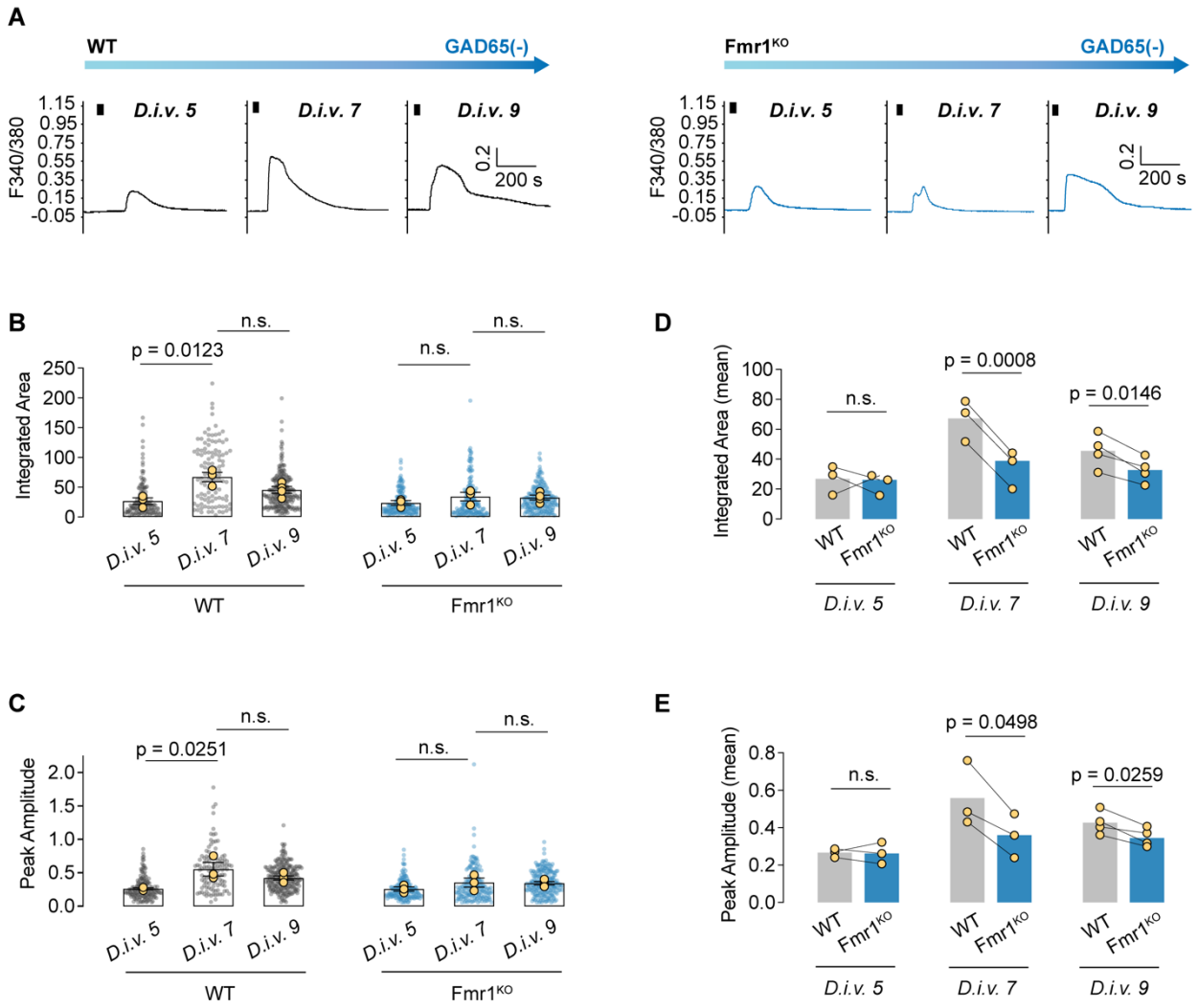

Fig. 3. Agonist-evoked α7 nAChR Ca^{2+} responses are dampened in *Fmr1*^{KO} glutamatergic neurons during early neuronal maturation. (A) Representative traces of Ca^{2+} responses evoked by 100 nM PNU-282987/3 µM PNU-120596 (black bars) in WT (left) and *Fmr1*^{KO} GAD65(-) glutamatergic neurons (right) during maturation in vitro (d.iv. 5, 7, 9). (**B**) Quantification of the integrated area of the response over time in GAD65(-) neurons. Yellow symbols represent the means of individual experiments (N = 3 for d.i.v. 5 and 7, N =4 for d.i.v. 9), filled symbols correspond to all measured responses (WT, d.i.v. 5 n = 139, d.i.v. 7 n = 112, d.i.v. 9 n = 231; *Fmr1*^{KO} d.i.v. 5 n = 172, d.i.v. 7 n = 170, d.i.v. 9 n = 216); one way ANOVA with Tukey's post test per group, WT p = 0.0123, KO p = 0.3743. (**C**) Quantification of peak amplitude over time in GAD65(-) neurons. Yellow symbols, experimental means (N = 3 for d.i.v. 5 and 7, N = 4 for d.i.v. 9); filled symbols, all measured responses (WT, d.i.v. 5 n = 148, d.i.v. 7 n = 115, d.i.v. 9 n = 232; *Fmr1*^{KO} d.i.v. 5 n = 176, d.i.v. 7 n = 180, d.i.v. 9 n = 219); one way ANOVA with Tukey's post test per group, WT p = 0.0302, KO p = 0.3018. (**D**) Paired comparison between WT and *Fmr1*^{KO} GAD65(-) neurons of mean integrated area of Ca^{2+} responses at different ages in vitro in matched cultures. Mean ± SEM, d.i.v. 5 WT 26.8 ± 5.63 KO 23.7 ± 4.0 N = 3, d.i.v. 7 WT 67.2 ± 8.04 KO 34.4 ± 7.26 N =3, d.i.v. 9 WT 45.5 ± 5.73 KO 32.7 ± 4.21 N = 4; paired t test. (**E**) Paired comparison between WT and *Fmr1*^{KO} GAD65(-) neurons of mean peak amplitude of Ca^{2+} responses at different ages in vitro in matched cultures. Mean ± SEM, d.i.v. 5 WT 0.27 ± 0.014 KO 0.26 ± 0.033 N = 3, d.i.v. 7 WT 0.56 ± 0.1 KO 0.36 ± 0.068 N =3, d.i.v. 9 WT 0.43 ± 0.031 KO 0.35 ± 0.025 N = 4; paired t test.

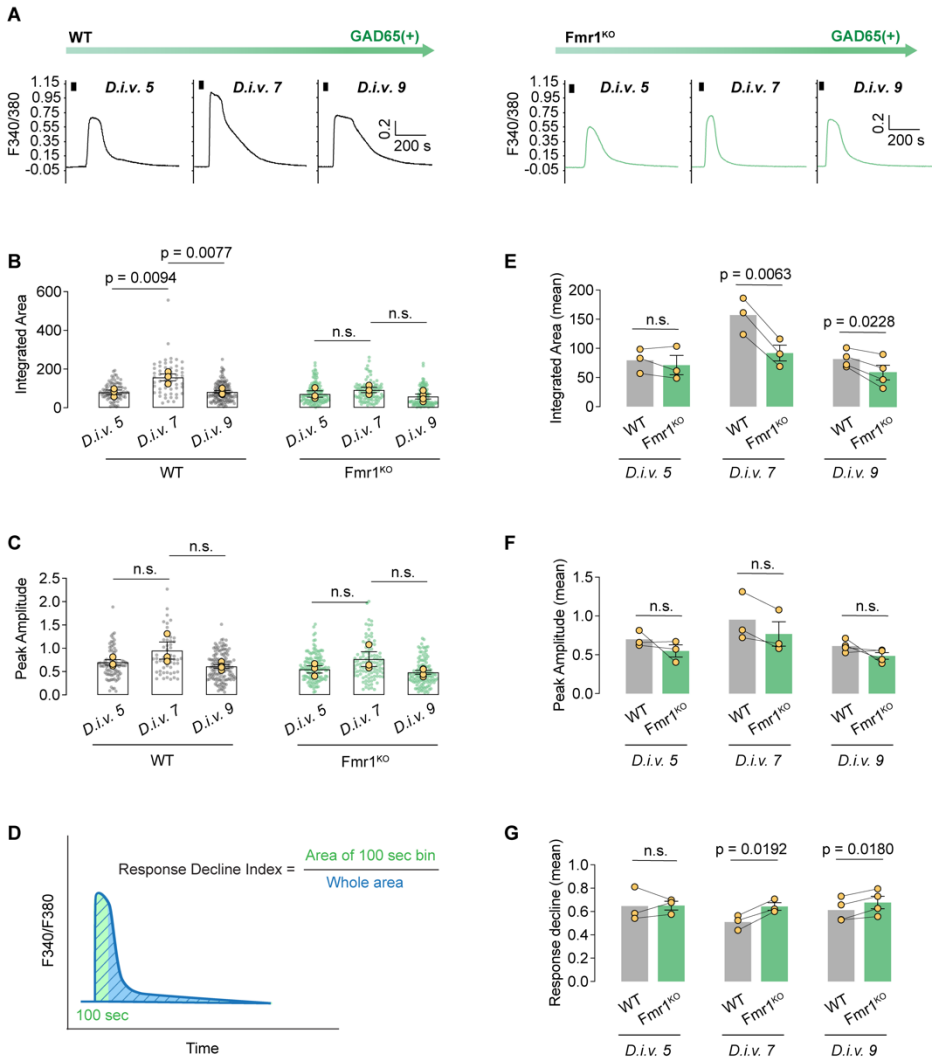

Fig. 4. Agonist-evoked α7 nAChR Ca^{2+} responses are dampened in *Fmr1*^{KO} GABAergic cells during early neuronal maturation. (A) Representative traces of Ca^{2+} responses evoked by 100 nM PNU-282987/3 μM PNU-120596 (black bars) in WT (left) and *Fmr1*^{KO} (right) GAD65(+) GABAergic cells during maturation in vitro (d.iv. 5, 7, 9). (**B**) Quantification of the integrated area of the response over time in WT and *Fmr1*^{KO} GAD65(+) neurons. Yellow symbols are means of individual experiments (N = 3 for d.i.v. 5 and 7, N =4 for d.i.v. 9), filled symbols correspond to all measured responses (WT, d.i.v. 5 n = 85, d.i.v. 7 n = 54, d.i.v. 9 n = 135; *Fmr1*^{KO} d.i.v. 5 n = 126, d.i.v. 7 n = 99, d.i.v. 9 n = 116); one way ANOVA with Tukey's post test per group, WT p = 0.0053, KO p = 0.2982. (**C**) Quantification of peak amplitude across ages in WT and *Fmr1*^{KO} GAD65(+) neurons. Yellow symbols, experimental means (N = 3 for d.i.v. 5 and 7, N = 4 for d.i.v. 9); filled symbols, all measured responses (WT, d.i.v. 5 n = 87, d.i.v. 7 n = 54, d.i.v. 9 n = 136; *Fmr1*^{KO} d.i.v. 5 n = 128, d.i.v. 7 n = 101, d.i.v. 9 n = 117); one way ANOVA with Tukey's post test per group, WT p = 0.1168, KO p = 0.1563. (**D**) Schematic trace illustrating the response decline index used for comparison of response duration across groups. (**E**) Paired comparison between WT and *Fmr1*^{KO} GAD65(+) neurons of mean integrated area at different ages in vitro in matched cultures. Mean ± SEM, d.i.v. 5 WT 79.5 ± 12.1 KO 71.3 ± 16.6 N = 3, d.i.v. 7 WT 157 ± 18.1 KO 91.9 ± 13.6 N =3, d.i.v. 9 WT 81.7 ± 7.42 KO 58.4 ± 12.6 N = 4; paired t test. (**F**) Paired comparison between WT and *Fmr1*^{KO} GAD65(+) neurons of mean peak amplitude at different ages in vitro in matched cultures. Mean ± SEM, d.i.v. 5 WT 0.7 ± 0.059 KO 0.55 ± 0.078 N = 3, d.i.v. 7 WT 0.95 ± 0.18 KO 0.77 ± 0.16 N =3, d.i.v. 9 WT 0.61 ± 0.038 KO 0.49 ± 0.042 N = 4; paired t test. (**G**) Paired comparison of response duration in matched cultures measured by response decline index. Mean ± SEM, d.i.v. 5 WT 0.65 ± 0.084 KO 0.65 ± 0.038 N = 3, d.i.v. 7 WT 0.51 ± 0.037 KO 0.64 ± 0.032 N =3, d.i.v. 9 WT 0.61 ± 0.05 KO 0.68 ± 0.053 N = 4; paired t test.

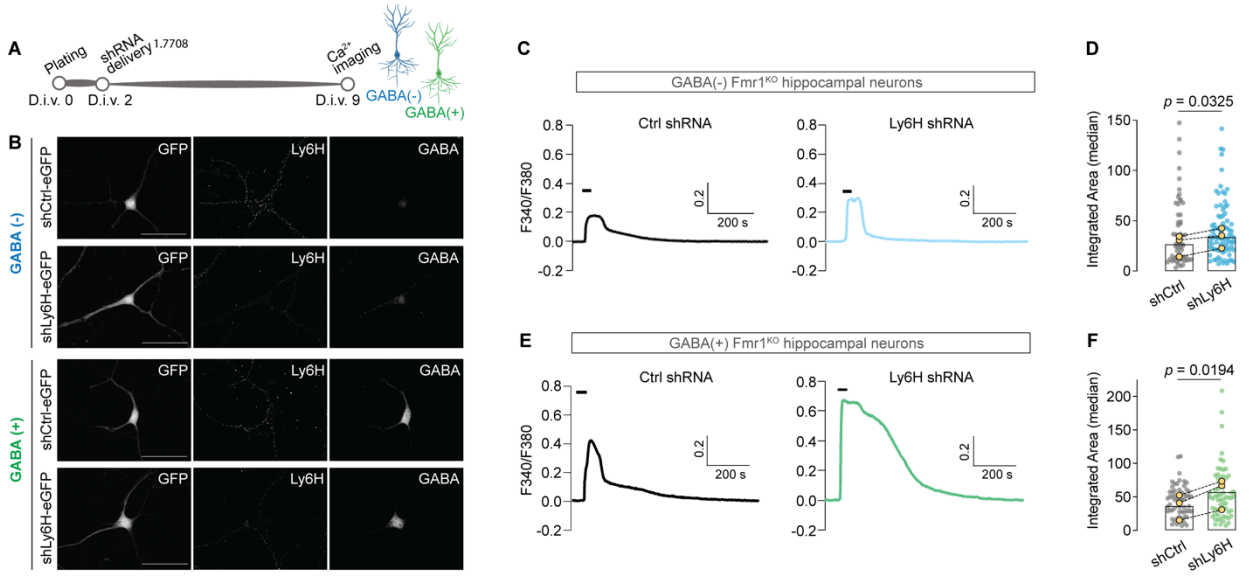

Fig. 5. Ly6H knockdown in *Fmr1*^{KO} hippocampal neurons potentiates evoked α7 nAChR Ca^{2+} responses. (A) Schematic of experimental strategy. **(B)** Representative images of *Fmr1*^{KO} hippocampal neurons (d.i.v. 9) transduced with Ly6H shRNA (shLy6H) or scrambled shRNA (shCtrl) and co-expressing eGFP (GFP). Cells were immunolabeled after Ca^{2+} imaging (post-hoc) for Ly6H and GABA; scale bars, 50 µm. (**C**) Representative traces of Ca^{2+} responses induced by 100 nM PNU-282987/3 µM PNU-120596 (black bars) in d.i.v. 9 GABA(-) neurons infected with shLy6H or shCtrl. **(D)** Quantification of the integrated area of the response in GABA(-) neurons; filled symbols represent all measured responses (shLy6H n = 86), shCtrl n = 60), yellow symbols are the response medians of N = 3 independent experiments; paired t test. (**E**) Representative traces of responses evoked as in (C) in GABA(+) *Fmr1*^{KO} neurons at d.i.v. 9 treated with shLy6H or shCtrl. (**F**) Quantification of the integrated area in GABA(+) neurons; filled symbols represent all measured responses (shLy6H n = 64, shCtrl n = 60), yellow symbols are the response medians of N = 3 experiments; paired t test.

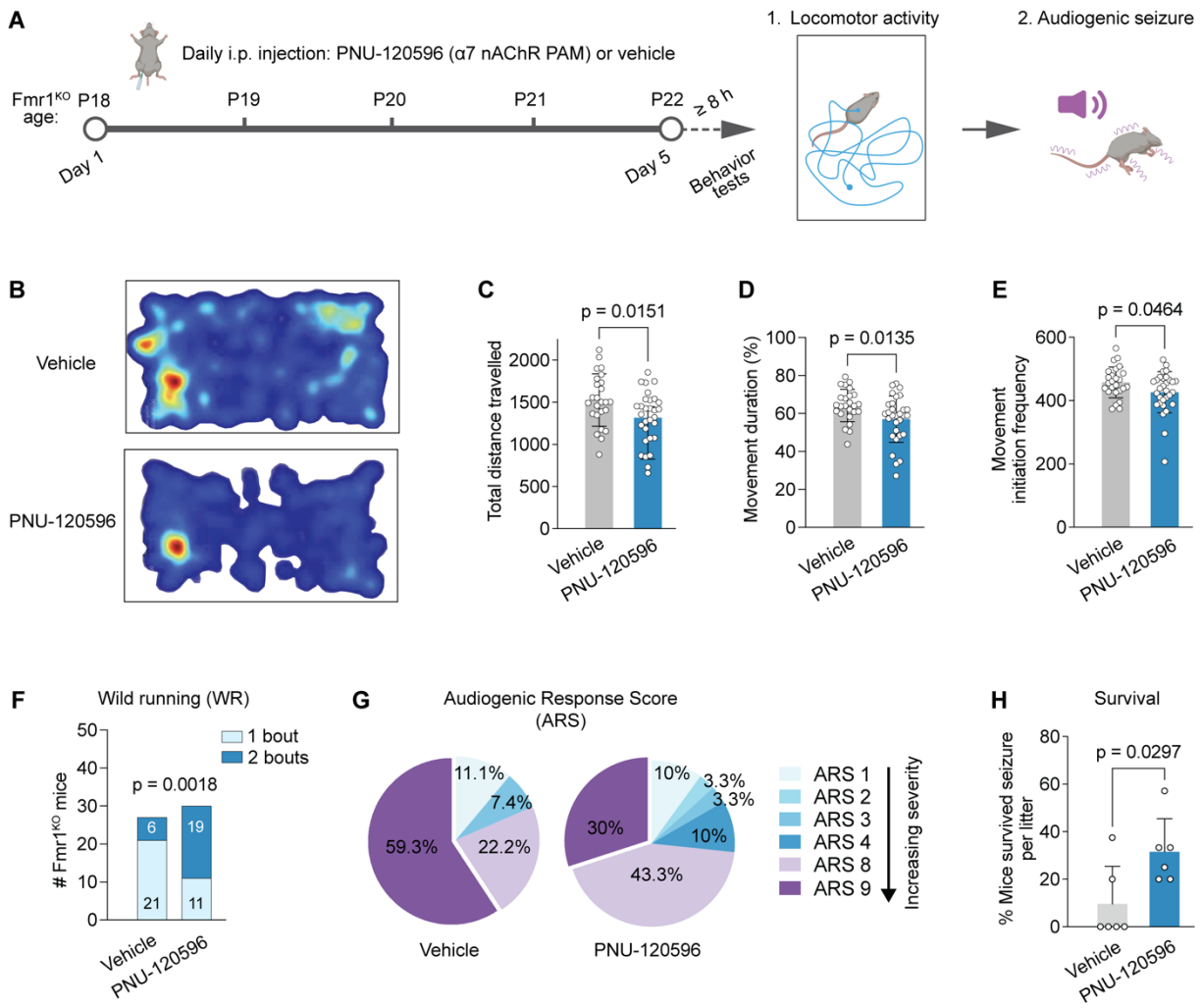

Fig. 6. PNU-120596 decreases hyperactivity and seizure severity in *Fmr1*^{KO} mice. (A) Schematic of experimental strategy and timeline; created with Biorender. (**B**) Representative activity heatmap from analysis of the videorecorded behavior of *Fmr1*^{KO} mice treated with the α7 nAChR PAM PNU-120596 (3 mg/kg) or vehicle. (**C**) Quantification of total distance traveled; mean ± SEM, vehicle 1527 ± 62 cm n = 25 mice, PAM 1315 ± 57 n =30, unpaired t test with Welch correction. (**D**) Quantification of percentage of time spent in movement; mean ± SEM, vehicle 64 ± 1.7 n = 25 mice, PAM 57 ± 2.2 n =30, unpaired t test with Welch correction. (**E**) Quantification of the frequency of movement initiation; mean ± SEM, vehicle 458 ± 9.7 n = 25 mice, PAM 426 ± 12 n =30, unpaired t test with Welch correction. (**F**) Analysis of audiogenic seizure severity; number of *Fmr1*^{KO} mice treated with vehicle or PAM exhibiting one bout of wild running (WR1) versus two (WR2); vehicle n = 27 mice tested, PAM n = 30, Chi-square two-sided. (**G**) Percentage of *Fmr1*^{KO} mice treated with vehicle (n = 27) or PAM (n = 30) scoring in respective category of the Audiogenic Response Score (ARS); only observed ARS categories are displayed. A larger number of vehicle-treated mice experienced seizures with ARS9 vs 8, compared to those treated with PAM: p = 0.0331, Chi-square two-sided. (**H**) Percentage per litter of vehicle and PAM-treated *Fmr1*^{KO} mice that survived after seizure; mean ± SEM, vehicle 9.6 ± n = 6.5, PAM 31 ± n = 5.7 n=6 litters, unpaired t test with Welch correction.

Funding:

National Institutes of Health grant U54 HD090260 (Walkley SU, PI); IDDRC Pilot Project (AF)

National Institutes of Health grant MH108614 (AF)

National Institutes of Health grant S10OD025295 (Instrumentation grant; Dobrenis K, PI)

Author contributions:

Conceptualization: SG, VKV, AF

Methodology: SG, DCM, VKV, AF

Investigation: SG, DCM, AF

Visualization: SG, VKV, AF

Funding acquisition: VKV, AF

Project administration: AF

Supervision: VKV, AF

Writing – original draft: SG

Writing – review & editing: SG, VKV, AF

Competing interests:

Authors declare that they have no competing interests.

Data and materials availability:

All data are available in the main text or the supplementary materials.

Supplementary Figures

Goebel et al.

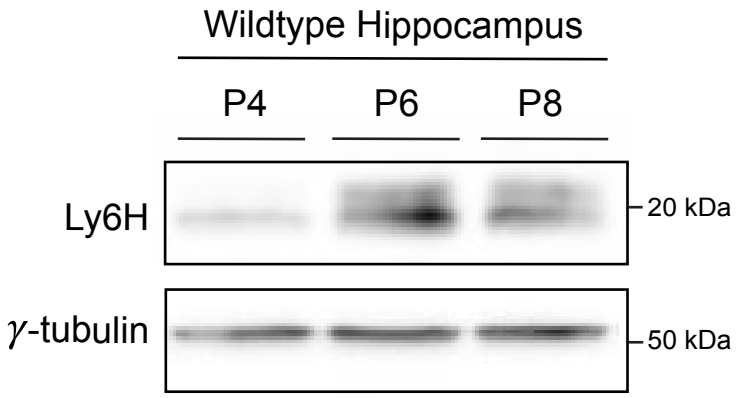

Fig. S1. Ly6H protein expression during hippocampal early postnatal development. Representative Western blot of hippocampal tissue lysates probed for Ly6H and γ-tubulin (loading control) in wild type mice at P4, P6, and P8

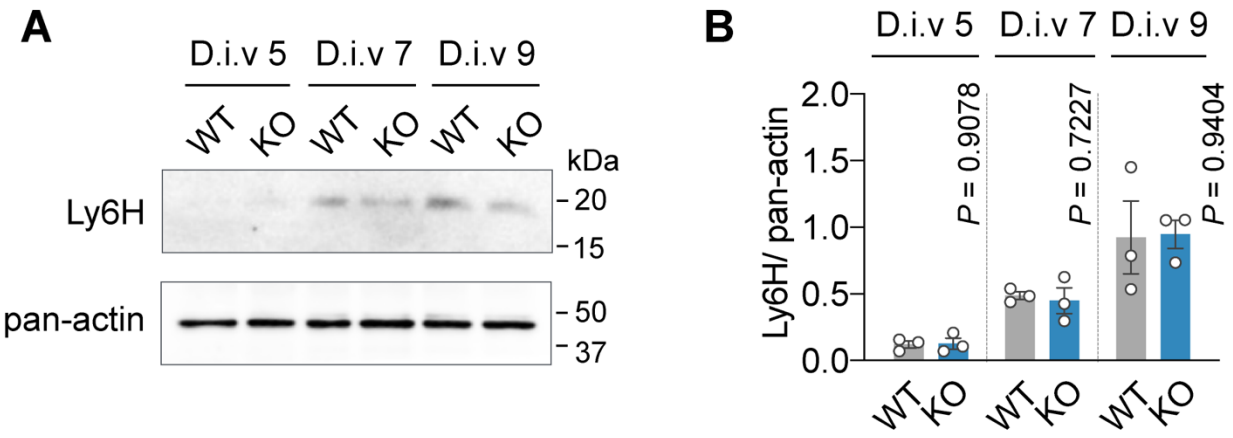

Fig. S2. The total abundance of Ly6H is not altered in *Fmr1*^{KO} hippocampal neurons. (A) Western blot of extracts from WT and *Fmr1*^{KO} hippocampal neurons at different ages in vitro probed for Ly6H and pan-actin (loading control). (**B**) Quantification of Ly6H abundance relative to actin; mean ± SEM, WT d.i.v. 5 0.121 ± 0.0265, d.i.v. 7 0.487 ± 0.0291, d.i.v. 9 0.924 ± 0.273, KO d.i.v. 5 0.127 ± 0.0414, d.i.v. 7 0.449 ± 0.0962, d.i.v. 9 0.947 ± 0.106, n = 3, unpaired t test.

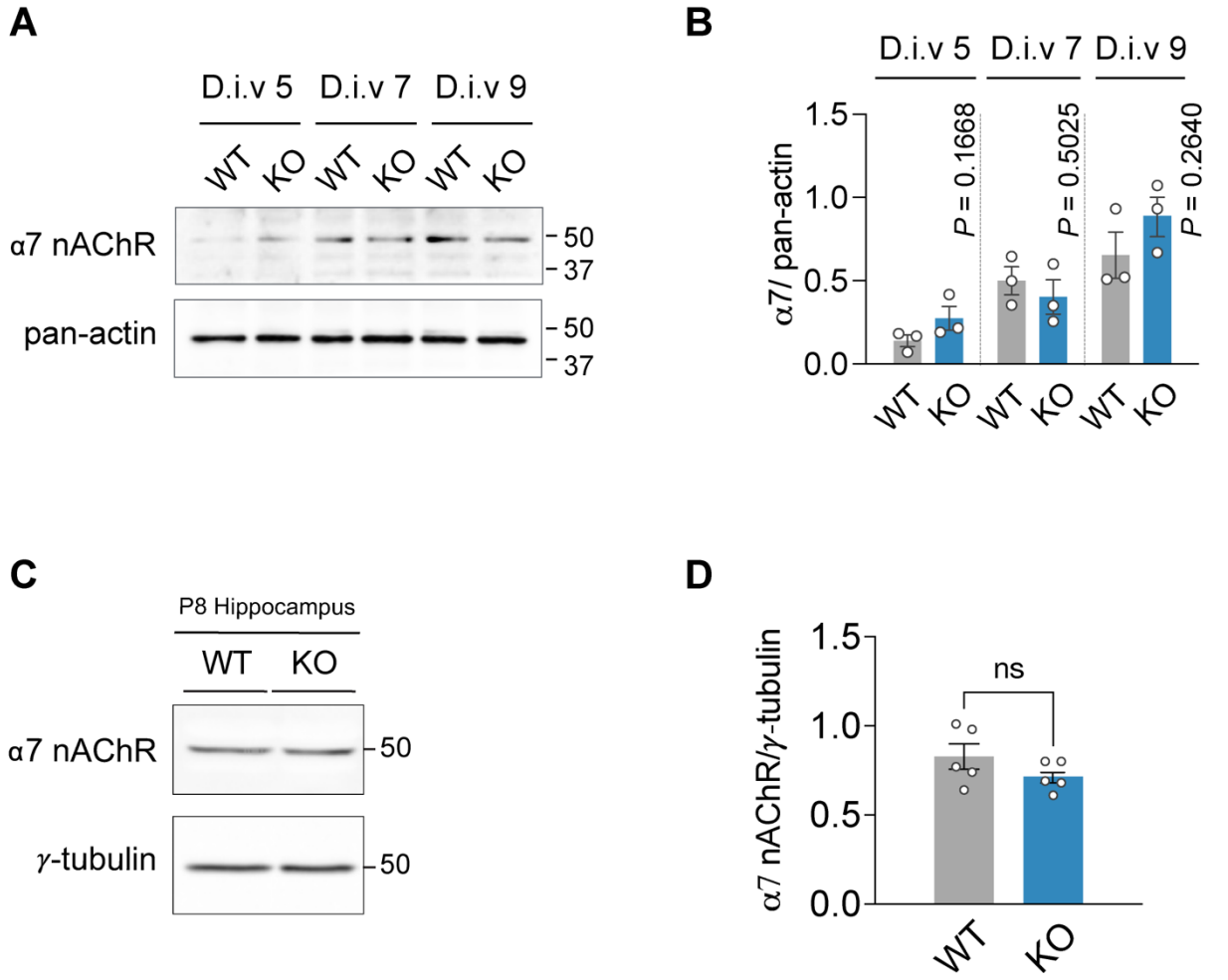

Fig. S3. α7 subunit expression is not altered in *Fmr1*^{KO} mice. (A) Western blot of extracts from WT and *Fmr1*^{KO} hippocampal neurons at different ages in vitro probed for α7 subunit and pan-actin (loading control, same as in fig. S2). (**B**) Quantification of α7 subunit abundance relative to actin; mean ± SEM, WT d.i.v. 5 0.14 ± 0.035, d.i.v. 7 0.5 ± 0.084, d.i.v. 9 0.654 ± 0.139, KO d.i.v. 5 0.275 ± 0.0717, d.i.v. 7 0.402 ± 0.103, d.i.v. 9 0.891 ± 0.118, n = 3, unpaired t test. (**C**) Western blot of extracts from WT and *Fmr1*^{KO} P8 hippocampus probed for α7 subunit and tubulin (loading control). (**D**) Quantification of α7 subunit abundance relative to tubulin in WT and *Fmr1*^{KO} mice; mean ± SEM, WT 0.828 ± 0.0717, KO 0.716 ± 0.037, n = 5 mice/genotype, p = 0.2022, unpaired t test.

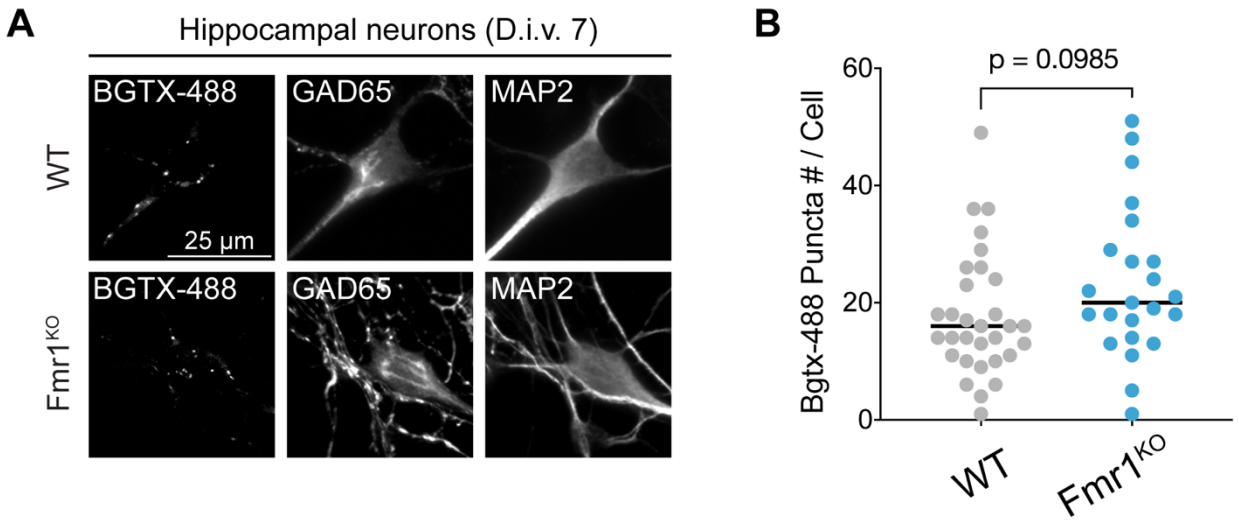

Fig. S4. Expression of BGTX-labeled mature α7 nAChRs is not altered in *Fmr1*^{KO} GABAergic cells. (A) Representative images of bound BGTX in non-permeabilized d.i.v. 7 hippocampal neurons labeled for GAD65 and MAP2; scale bar, 25 µm. (**B**) Quantification of BGTX labeled clusters in the somatodendritic region of WT and *Fmr1*^{KO} GAD65(+) neurons; WT n = 31 cells, KO n = 23 from 3 independent experiments, p = 0.0985, unpaired t test.

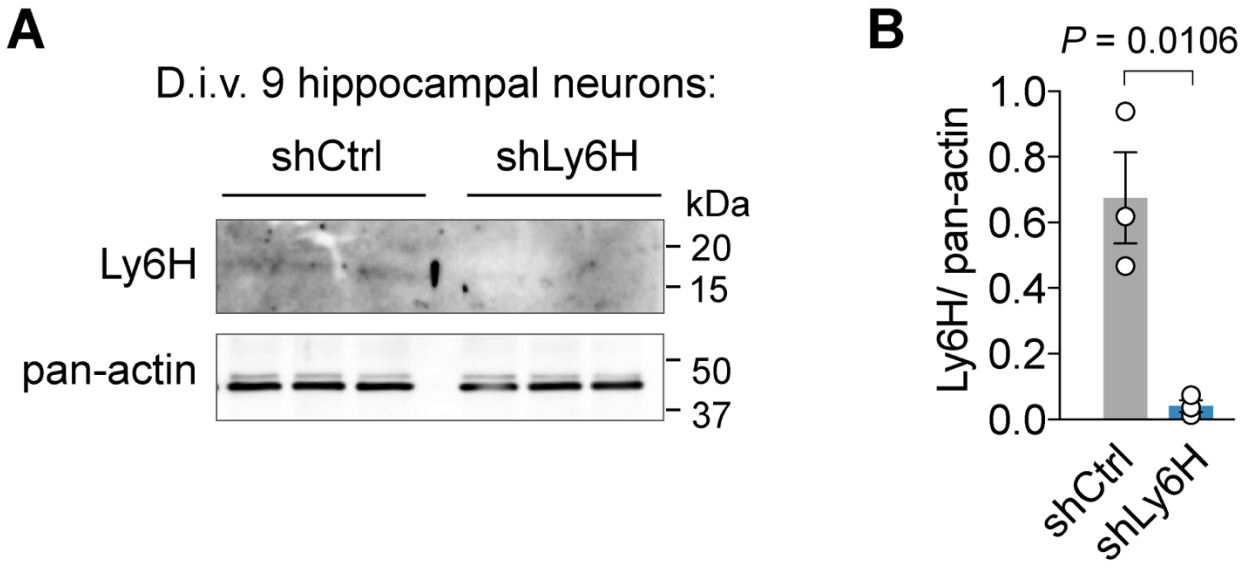

Fig. S5. Reduced expression of Ly6H in neurons transduced with Ly6H shRNA. (A) Western blot of extracts from hippocampal neurons transduced with control (shCtrl) or Ly6H shRNA (shLy6H) probed for Ly6H and pan-actin (loading control). (**B**) Quantification of Ly6H abundance relative to actin; mean ± SEM, control 0.68 ± 0.14, Ly6H shRNA 0.041 ± 0.018, n = 3, unpaired t test.

A

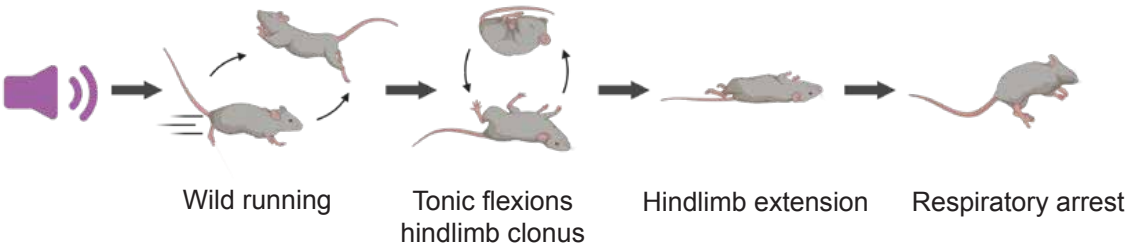

B

Audiogenic Response Score (ARS)

ARS 1	One bout of wild running (WR1)
ARS 2	Two bouts of wild running (WR2) and generalized clonus
ARS 3	WR1 and generalized clonus
ARS 4	WR2, tonic flexion of neck/trunk/forelimbs, clonus of hindlimbs
ARS 5	WR1, tonic flexion of neck/trunk/forelimbs, clonus of hindlimbs
ARS 6	WR2, tonic flexion of neck/trunk/forelimbs, hindlimb partial tonic extension
ARS 7	WR1, tonic flexion of neck/trunk/forelimbs, hindlimb partial tonic extension
ARS 8	WR2, tonic flexion of neck/trunk/forelimbs, hindlimb complete tonic extension
ARS 9	WR1, tonic flexion of neck/trunk/forelimbs, hindlimb complete tonic extension

Fig. S6. **Audiogenic Seizure Response Score**. (**A**) Illustration of the progression of audiogenic seizures: created with Biorender. (**B**) Description of Audiogenic Response Score (ARS) criteria used in the study.